Characterization of Target Gene Regulation by the Two Epstein-Barr Virus Oncogene LMP1 Domains Essential for B-cell Transformation

Bidisha Mitra[1-3], Rui Guo[1-3], Eric M. Burton[1-3], Laura A. Murray-Nerger[1-3] and Benjamin E. Gewurz[1-3,5*]

[1] Division of Infectious Diseases, Department of Medicine, Brigham and Women's Hospital, 181 Longwood Avenue, Boston MA 02115, USA
[2] Center for Integrated Solutions in Infectious Disease, Broad Institute of Harvard and MIT, Cambridge, MA 02142, USA
[3] Department of Microbiology, Harvard Medical School, Boston, Massachusetts 02115, USA
*Correspondence: bgewurz@bwh.harvard.edu

Abstract:

The Epstein-Barr virus oncogene latent membrane protein 1 (LMP1) is expressed by multiple EBV-associated malignancies, where it mimics CD40 signaling to activate growth and survival pathways. Two LMP1 cytoplasmic tail domains are essential for EBV-driven transformation of human B lymphocytes into immortalized lymphoblastoid cell lines (LCL), a model for EBV+ lymphomas of immunosuppressed hosts. Classic genetic studies defined two LMP1 C-terminal cytoplasmic tail regions, termed transformation essential sites (TES) 1 and 2, as critical for B-cell transformation. However, a longstanding question has remained how TES1 and TES2 non-redundantly versus jointly regulate key target genes. To gain insights, we conditionally expressed wildtype LMP1 versus LMP1 point mutants abrogated for TES1 and/or TES2 signaling in Burkitt B-cells with low basal NF-kB activity. RNAseq analyses revealed gene clusters that responded more strongly to TES1 versus TES2, that respond strongly to both, or that are oppositely regulated by TES1 and 2. Cross-comparison with EBV-transformed B-cell CRISPR/Cas9 screens identified TES1 and 2 effects on genes critical for LCL growth and survival, including BATF and IRF4. Similarly, bioinformatic analysis highlighted TES1 vs TES2 roles in regulation of genes targeted by EBV super-enhancers, which in LCLs are bound by all 5 NF-kB transcription factors. To further identify key LMP1 targets, we profiled LCL transcriptome-wide responses to CRISPR LMP1 knockout. Collectively, these studies suggest a model by which LMP1 TES1 and TES2 jointly remodel the B-cell transcriptome to support oncogenic growth and survival.

Key Words: gammaherpesvirus; lymphoproliferative disease; tumor virus; B-cell oncogenesis; interferon regulatory factor; BATF; NF-kB; super-enhancer; dependency factor.

Short title: The LMP1 TES1 and TES2 host target gene landscape

Introduction:

Epstein-Barr virus (EBV) is a gamma-herpesvirus that persistently infects most adults worldwide. EBV causes 200,000 cancers per year, including Burkitt lymphoma, Hodgkin lymphoma, post-transplant lymphoproliferative disease (PTLD), and HIV/AIDS associated lymphomas. EBV also causes a range of epithelial cell tumors, including gastric and nasopharyngeal carcinomas, as well as T and NK cell lymphomas(1). The key EBV oncogene latent membrane protein 1 (LMP1) is expressed in most of these tumors, where it drives growth and survival pathway signaling.

To colonize the B-cell compartment and establish lifelong infection, EBV uses a series of viral latency genome programs, in which different combinations of latency genes are expressed. These include six Epstein-Barr nuclear antigens (EBNA) and the membrane oncoproteins LMP1, LMP2A and LMP2B. LMP1 mimics aspects of signaling by the B-cell co-receptor CD40 (2-5), whereas LMP2A rewires surface B-cell immunoglobulin receptor signaling (6). All nine latency oncoproteins are expressed in the EBV B-cell transforming latency III program, which are expressed in immunoblastic lymphomas of immunosuppressed hosts. These include PTLD and primary central nervous system lymphoma. The latency II program is observed in EBV+ Hodgkin lymphoma, where the Reed-Sternberg tumor cells express EBNA1, LMP1 and LMP2A. Latency II is also frequently observed in T and NK cell lymphomas and in nasopharyngeal carcinoma. Host genome NF-κB activating mutations are frequently observed in EBV-negative Hodgkin lymphoma, but to a much lesser extent in EBV+ tumors, underscoring LMP1's key role in activating growth and survival signaling (7).

LMP1 localizes to lipid rafts, where it signals constitutively in a ligand-independent fashion to activate NF-κB, MAP kinase, STAT3, PI3K, interferon and P62 pathways. LMP1 is comprised of a short N-terminal cytoplasmic tail, six transmembrane (TM) domains and a 200 residue C-terminal cytoplasmic tail (2-5). LMP1 TM domains drive homotypic aggregation, lipid raft association and constitutive signaling (8, 9). The LMP1 C-terminal tail functionally mimics signaling from activated CD40 receptors, to the point that the CD40 tail can essentially be replaced by LMP1's in transgenic mice studies. However, while CD40/LMP1 knockin mice had relatively normal B-cell development and evidence of intact CD40 function, including germinal center formation and class switch recombination, T-cell independent B-cell activation was also observed (10). These experiments suggest that the LMP1 C-terminal tail mimics CD40 signaling, but has also evolved additional functions.

Reverse genetic studies identified two LMP1 C-terminal cytoplasmic tail domains that are critical for EBV-mediated conversion of primary human B-cells into immortalized, continuously growing lymphoblastoid cell lines (LCL). Transformation effector site 1 (TES1), also called C-terminal activating region 1 (CTAR1), spans LMP1 residues 186-231. TES1/CTAR1 contains a PXQXT motif that engages tumor necrosis factor receptor associated factors (TRAFs). TES1 activates canonical NF-κB, non-canonical NF-κB, MAP kinase, PI3K and STAT3 pathways (3, 4, 11-15). TES2, which spans residues 351-386 and is also referred to as CTAR2, activates canonical NF-κB, MAPK, IRF7 and P62 pathways (3-5, 16-20). TRAF6 is critical for LMP1 TES2-driven canonical NF-κB, MAPK and p62 pathway activation (21-26). Canonical NF-□B signaling is critical for TES2/CTAR2 driven target gene regulation in a 293 cell conditional expression model (27). Signaling from a third LMP1 C-terminal tail region, CTAR3, activates JAK/STAT and SUMOylation pathways (28-30) potentially important *in vivo* but that are not essential for EBV-driven B-cell transformation (31). ChIP-seq analyses

demonstrated a complex NF-κB binding landscape in LCLs, in which constitutive LMP1 signaling stimulates different combinations of the NF-κB transcription factors RelA, RelB, cRel, p50 and p52 to bind B-cell enhancers and promoters (32).

LMP1 is the only EBV oncogene that can independently transform rodent fibroblasts, driving anchorage independent growth and loss of contact inhibition (33-35). LMP1 expression drives aberrant B-cell growth in transgenic B-cell models, particularly in combination with LMP2 upon disruption of cell mediated immunity (36-39). While not critical for the first 8 days of EBV-driven B-cell outgrowth (40), LMP1 is critical for EBV-mediated conversion of primary human B-cells into immortalized LCLs (41, 42). A longstanding question has remained why TES1 and TES2 are each essential for EBV-mediated LCL establishment. Experiments using the EBV second site mutagenesis method (43) demonstrated that TES1 is critical for initiation of EBV-infected lymphoblastoid cell outgrowth (44). By contrast, TES2 is critical for long-term LCL growth, although TES2 null EBV infected lymphoblastoid cells could be propagated on epithelial feeders (44, 45). It remains incompletely understood why TES1 and TES2 are each therefore important for EBV-driven B-cell growth transformation.

To gain insights into non-redundant, additive or synergistic roles, we constructed Burkitt B-cell models with conditional expression of wildtype, TES1 mutant, TES2 mutant or TES1/2 double mutant LMP1. RNAseq profiling identified multiple modes of target gene regulation in response to LMP1 signaling, providing new insights into independent versus shared TES1 and 2 roles. Cross-comparison with CRISPR screen defined dependency factors identified a subset of LMP1 target genes critical for LCL proliferation. Similarly, differential TES1 and TES2 contributions to the regulation of genes targeted by viral super-enhancers were identified.

Results:

RNAseq identifies clusters of host genes that respond differentially to LMP1 signaling

To characterize LMP1 B-cell genome-wide targets, we established Akata or BL-41 Burkitt cells with doxycycline inducible wildtype (WT) LMP1 expression. Importantly, these Burkitt cell lines have relatively low basal NF-κB activity levels. We also established Akata or BL-41 with conditional LMP1 point mutants that abrogate signaling from TES1 (TES1m, 204PQQAT208 -> AQAAT) or TES2 (TES2m, 384YYD386 -> ID) (45-47). For cross-comparison, we also established conditional TES1/TES2 double mutant (DM) cell lines with both mutations, to profile responses to other LMP1 regions, potentially including CTAR3 or unfolded protein responses induced by LMP1 induction (48, 49) (**Fig. 1A**). WT and point mutant LMP1 were expressed to similar extents across the panel. As expected, TES1m and DM exhibited impaired non-canonical NF-κB pathway activation, as judged by p100:p52 processing (**Fig S1A-B**). LMP1 signaling across Akata and BL-41 cell lines was also confirmed by FACS analysis of ICAM-1 and Fas upregulation (**Fig. S1C-J**).

We first profiled LMP1 effects on EBV- Akata cells (50) using RNA-seq analysis. K-means analysis with n=6 clusters was used to visualize effects of LMP1 induction on genome-wide host gene expression. This analysis revealed strikingly distinct patterns of host gene responses to WT, TES1m, TES2m and DM LMP1 (**Fig. 1B, Table S1.1-4**). Cluster 1 genes were highly upregulated by WT LMP1, to a lesser extent by TES2m (in which only TES1 signals), and more modestly by TES1m (in which only TES2 signals). This result suggests that TES1 signaling is likely important for their induction, whereas TES1 and TES2 can then additively or synergistically upregulate these genes. Kyoto Encyclopedia of Genetic Elements (KEGG) gene ontology (GO) analysis identified enrichment of multiple inflammatory immune pathways amongst Cluster 1 genes, a representative subset of which are displayed in **Fig. 1C.** For instance, the interferon stimulated genes IFIT1 and CXCL9, the latter of which encodes a T-cell attracting chemokine, are observed as members of Cluster 1. KEGG pathways enriched amongst Cluster 1 genes included TLR signaling, chemokine signaling, IFN signaling and NLR signaling (**Fig. 1C, Table S4.26**). Cluster 1 also contained well described LMP1 target genes, including TRAF1, consistent with prior studies that found it to be predominantly TES1 induced (46) and have been validated by immunoblot (**Fig. S1A**). Notably, MAP3K7, which encodes the kinase TAK1 is also a Cluster 1 gene. Since TAK1 is critical for TES2/canonical NF-κB and MAP kinase signaling (26), this result suggests an important mechanism of cross-talk between TES1 and TES2. Likewise, the Cluster I gene IRF7 binds to and is activated by TES2 (51-54) again suggesting cross-talk between LMP1 pathways. STAT1 and STAT3 are also Cluster 1 genes, raising the question of whether these STATs may drive interferon stimulated gene induction downstream of LMP1.

Cluster 2 genes were induced by WT, TES1m or TES2m LMP1 to a similar extent (**Fig. 1B**), suggesting that they redundantly respond to TES1 or TES2 signaling. GO analysis highlighted enrichment of NF-κB signaling in this cluster, and which included mRNAs encoding four NF-κB transcription factor subunits, as well as the NF-κB induced inhibitors IκBα, IκBδ and IκBε. mRNA fold changes for *NFBK2*, which encodes non-canonical pathway NF-κB p52 transcription factor and for CD40 are shown in **Fig. 1D (Table S4.26)**. Consistent with a prior study (46), Fas and ICAM-1 are Cluster 2 genes similarly induced on the mRNA level by TES1m and TES2m, though interestingly, plasma membrane ICAM-1 levels were lower in cells expressing TES1m

(**Fig. S1C-F**). This result raises the possibility that TES1 signaling may play a role in ICAM-1 post-transcriptional regulation and/or trafficking.

Cluster 3 genes were expressed at lower levels in cells expressing TES1m, even as compared with cells expressing LMP1 DM, suggesting that unopposed TES2 signaling results in their downregulation (**Fig. 1B, S2A**). GO analysis highlighted enrichment for multiple metabolism pathways amongst Cluster 3, including oxidative phosphorylation (**Fig. S2A**). This result suggests previously unrecognized TES1 and 2 roles in metabolism regulation. Cluster 4 contained a smaller subset of host genes, downregulated by TES1 signaling, including in the WT LMP1 context. This geneset was enriched for SNARE interactions in vesicular transport and sphingolipid metabolism (**Fig. S2B**). Cluster 5 mRNAs were instead upregulated by unopposed TES2 signaling (**Fig. 1B, S2C**) and enriched for ubiquitin mediated proteolysis, including Cullins Cul1-3. Finally, Cluster 6 genes were repressed by TES1 and TES2 signaling in an additive manner (**Fig. 1B, E**). This geneset was enriched for mismatch and base excision repair, nucleotide metabolism, cystine and methionine metabolism (**Table S4.26)**. TES1 and TES2 signaling may additively recruit the same repressors or may instead recruit co-repressors to these sites.

We next used RNAseq to profile BL-41 Burkitt cells, which are derived from an EBV-negative sporadic Burkitt lymphoma tumor (55). Notably, BL-41 express higher basal ICAM-1 and Fas than Akata, suggesting that they may have somewhat higher NF-κB activity (**Fig. S1**). RNAseq was performed at 24 hours post-expression of WT, TES1m, TES2m or DM. K-means analysis with n=6 clusters again revealed categories of genes that respond differently to the LMP1 series (**Fig. S3A, Table S2.10-13**). Similar to Akata, Cluster 1 genes were most highly induced by WT, and to a lesser extent by TES1m or TES2m, suggesting that they are additively or synergistically induced by TES1/2. Cluster 1 genes included multiple chemokines, STAT1, IRF4, IRF5 and IRF9 (**Fig. S3A-B**). Again similar to what we observed in Akata, Cluster 2 genes were induced by TES1m and TES2m, but to a somewhat higher level by WT LMP1, suggesting partially redundant roles (**Fig. S3C**). BL-41 Cluster 4 genes were instead suppressed by unopposed TES1 signaling (**Fig. S3D**), whereas Cluster 6 genes were enriched for the antigen presentation pathway and were most highly induced by TES2m. These results suggest that TES1 may induce complexes that more weakly activate these targets (**Fig. S3E**). Differences in responses to LMP1 between Akata and BL-41 may likely reflect their somewhat distinct basal NF-κB levels, and likely also differences in pathways frequently found in EBV+ vs EBV- Burkitt lymphomas (56, 57). Nonetheless, both models highlight distinct clusters of host B-cell target genes that differ in responses to TES1, TES2 or combined TES1/2 signaling.

LMP1 WT, TES1, TES2 and DM target genes

We next cross-compared the most highly differentially-expressed genes across the LMP1 conditions. At a fold-change >2 and adjusted p value <0.05 cutoff, WT LMP1 highly upregulated 421 and downregulated 153 Akata genes, respectively. The most highly upregulated genes included multiple interferon stimulated genes, TRAF1, FAS and CFLAR, which encodes cFLIP (**Fig. 2A**, **Table S1.1**). Interestingly, WT LMP1 decreased expression of the recombinase RAG1 and RAG2 mRNAs, as well as MME, which encodes CD10, a plasma membrane protein that we and others have found is downmodulated by EBV latency III (58-60). GO analysis identified that WT LMP1 upregulated genes were significantly enriched for EBV infection (**Fig. 2B, Table**

S4.28), likely reflecting the major LMP1 contribution to latency III datasets used in KEGG, NF-κB and TLR signaling, whereas downmodulated genes were enriched in the term primary immunodeficiency. Similar effects were evident in the BL-41 cell context (**Fig. S4A-B**,**Table S2.10**).

To gain insights into how TES2 signaling shapes LMP1 genome-wide targets, we next cross-compared transcriptomes from Akata expressing WT vs TES1m. At a fold-change >2 and adjusted p value <0.05 cutoff, 96 genes were more highly expressed in WT than LMP1 TES1m, whereas 35 were less highly expressed. Interestingly, multiple interferon stimulated genes, including IFIT1, IFI6, STAT1 and IFI44 were amongst the most highly upregulated in WT LMP1 expressing cells (**Fig. 2C, Table S1.5**), whereas RAG2 and MME/CD10 were comparatively lower than in cells expressing TES1m. GO analysis identified TNF, Nod-like receptor (NLR) and JAK/STAT signaling to be enriched amongst genes more highly expressed in WT LMP1+ cells, whereas oxidative phosphorylation was the most highly enriched amongst genes more highly expressed in TES1m+ cells (**Fig. 2D, Table S4.28**). Similar analyses on BL-41 cell datasets again revealed large numbers of differentially expressed genes in WT vs TES1m LMP1 expressing cells (**Fig. S4C-D, Table S2.14**). Variances in basal NF-κB activity between Akata and BL-41, including baseline non-canonical NF-κB activity, may contribute to differences in these B cell contexts.

To then gain insights into how TES1 signaling shapes LMP1 genome-wide target gene effects, we cross-compared Akata differentially expressed genes at 24 hours post expression of WT vs TES2m LMP1. At a fold-change >2 and adjusted p value <0.05 cutoff, 193 genes were more highly expressed in WT than LMP1 TES1 expressing Akata, whereas 48 were less highly expressed. Once again, multiple interferon stimulated genes (ISG), including STAT1, IFI6 and OAS1 were more highly expressed in WT cells, whereas RAG1 was more highly expressed in TES2m expressing cells. GO analysis identified sphingolipid signaling and metabolism to be most highly enriched amongst WT LMP1 differentially upregulated genes, whereas TCA cycle was the most significant GO term amongst genes higher in LMP1 TES2m+ cells (**Fig. 2E-F, Table S1.6, Table S4.28**). Similar numbers of genes were differentially regulated between WT and TES2m expressing cells in the BL-41 context (**Table S2.15**), where Toll-like receptor signaling was the most highly enriched term amongst genes more highly expressed in WT LMP1+ cells (**Fig S4F)**. These analyses are consistent with a model in which TES1 and TES2 signaling additively or synergistically upregulate ISGs.

Cross-comparison of expression patterns in WT vs DM LMP1+ Akata or BL-41 cells identified a similar geneset to our comparison of WT vs uninduced cells (**Fig. 2G-H, S4G-H, Table S1.7, Table S2.16, Table S4.28, Table S4.29**). This result indicates that TES1 or TES2 signaling are necessary for most LMP1 effects on the Burkitt B-cell. Nonetheless, differences were observed, which may be explained by signaling from other LMP1 domains, including CTAR3, or by host cell responses to LMP1 expression, potentially including unfolded protein responses.

TES1 versus TES2 effects on host gene expression

Much remains to be learned about why LMP1 evolved two C-terminal tail domains essential for B-cell transformation. To characterize TES1 vs TES2 effects on the host B cell transcriptomic landscape, we next directly cross-compared LMP1 targets in Akata and BL-41.

While induction of WT or DM LMP1 had highly concordant effects in both Burkitt environments, there was substantially more variability TES1m and TES2m in these two Burkitt environments (**Fig. 3A-D**). Consistent with EBV's ability to infect B-cells at multiple stages of differentiation or activation, our result suggest that combined TES1 and TES2 signaling increase robustness of LMP1 signaling across distinct B-cell contexts. In the Akata environment, cells expressing TES2m more highly induced ISGs, including IFIT1, IFI6, OAS, IFI44 and DDX58 (**Fig. 3E, Table S1.8**). GO analysis indicated that Nod-like receptor (NLR), necroptosis and chemokine signaling pathways were enriched amongst genes more highly induced by TES2m, indicative of unopposed TES1 signaling. By contrast, amino acid metabolism was enriched amongst genes more highly induced by TES1m, indicative of unopposed TES2 signaling (**Fig. 3F, Table S4.30**). In the BL-41 context, interferon stimulated genes were not as highly induced by TES2m vs TES1m (**Fig. 3G, Table S2.17**). Since non-canonical NF-κB activity can strongly impact B cell type I interferon pathways (61), we suspect that differences in basal NF-κB activity in BL-41 may compensate to some extent to reduce this phenotype. Instead, cell adhesion molecules and TNF signaling were most highly enriched. For instance, CFLAR was significantly more highly induced by TES2m, as was OTULIN, a deubiquitinating enzyme that controls TNF/ NF-κB canonical pathway signaling. FoxO and Toll-like receptor signaling were the most highly enriched amongst TES1m upregulated BL-41 genes, with FOXO3B, FOXD1 and FOXC1 the most selectively induced (**Fig. 3H, Table S4.31**). GSEA analysis further highlighted pathways differentiated TES1m and TES2m cells (**Fig. S5, Table S3**).

CRISPR analysis of LCL LMP1 Target Genes

To further identify B-cell LMP1 target genes, we next investigated effects of CRISPR LMP1 knockout on LCL host and viral gene abundances. We used the well-characterized LCL GM12878, which is a Tier 1 Encode project cell line that we have used extensively for prior CRISPR analyses (25, 62). Cas9+ GM12878 were transduced with a lentivirus expressing a single guide RNA (sgRNA) targeting LMP1. Immunoblot confirmed efficient LMP1 depletion by 48 hours post-puromycin selection of transduced cells (**Fig. 4A**). LMP1 editing rapidly downmodulated LMP1/ NF-κB target genes, including p100/52, TRAF1 and IRF4 (**Fig. 4A**), but not GAPDH. At this early timepoint post-CRISPR editing, LCLs remained viable (**Fig. S6A**), whereas LMP1 knockout LCLs undergo growth arrest and cell death thereafter. We therefore used RNAseq to cross-compare the LCL transcriptome in cells expressing control versus LMP1 targeting sgRNA at this early timepoint. At a cutoff of adjusted p-value <0.05 and fold change of >2,351 host genes significantly changed in response to LMP1 editing, respectively. Differentially expressed genes could be broadly characterized into two k-means clusters of roughly equal size (**Fig. 4B, Table S1.9**). As examples of cluster 1, IRF4 and TNFRSF12A mRNAs were downmodulated by LMP1 depletion, whereas the cluster 2 genes OGDHL and CBS were instead highly upregulated (**Fig. 4C-D**).

GSEA analysis identified cytokine receptor signaling, NF-κB signaling and TNF signaling as enriched amongst genes downmodulated with LMP1 depletion (**Fig. 4E, Table S4.32)**. This nicely inversely correlates with GSEA analysis of WT LMP1 expression in Burkitt cells (**Fig. 2A**), suggesting on-target CRISPR effects on LMP1, and that LMP1 loss did not cause widespread host gene deregulation at this early timepoint. Interestingly, regulation of autophagy, TCA-cycle and HIF-1 signaling were enriched amongst cluster 2 genes upregulated in response to LCL LMP1 KO (**Fig. 4E**). We next directly cross-compared effects of GM12878 LMP1 knockout

versus WT LMP1 induction on host mRNA abundances (**Fig. 4F**). Volcano plot analysis highlighted TRAF1, EBI3, CCL2 and CD40 as amongst the most downregulated host genes upon LMP1 editing, consistent with prior studies (27, 46, 63-67) and with our Burkitt LMP1 studies that highlighted these as LMP1 targets (**Fig. 4G orange circles, Table S1.1&9**). We also identified a class of host genes that are upregulated by LCL LMP1 KO, but downregulated by Akata LMP1 WT expression (**green circles, Fig 4H**). Similar cross-comparison with Akata induced for TES1m or TES2m suggested subsets of these genes regulated by TES1 and/or TES2 signaling (**Fig. S6B-C**).Taken together, these findings serve to validate a class of host genes as LMP1 targets in the LCL context, although we cannot exclude that they are regulated through secondary effects.

Little has remained known about how LMP1 cross-regulates other EBV latency III genes. We therefore mapped RNAseq effects onto GM12878 EBV transcripts, and found that LMP1 depletion significantly downmodulated EBNA3A, 3C and EBNA-LP, though curiously not EBNA3C or EBNA2 (**Fig. 4H**). LMP1 regulates its own expression (68, 69), but we did not observe changes in LMP1 expression at the mRNA level. We note that CRISPR editing often results in insertions or deletions, causing functional protein knockout without necessarily changing mRNA levels of the edited gene. However, it is plausible a compensatory response to LMP1 knockout occurred on the mRNA level at this early timepoint, potentially balancing loss of NF-κB induced LMP1.

To gain further insights into LMP1 target genes that are mediators of LCL growth and survival, we cross compared LMP1 KO RNAseq data with our prior CRISPR analysis of host factors essential for LCL but not Burkitt growth and survival (25). This analysis identified that mRNA abundances of 37 of the 87 CRISPR-defined LCL selective dependency factors significantly changed in response to LMP1 KO (**Fig. 4I**). Of these, MDM2, BATF and NFKB2 were the most highly downregulated by LMP1 KO (**Fig, S6D**). STRING analysis suggested that LMP1-regulated LCL dependency factors may assemble into a network (**Fig. 4J**).

LMP1 TES1 and TES2 roles in LCL Dependency Factor BATF and IRF4 Expression

We next characterized LMP1 pathways important for BATF and IRF4 induction, given their key LCL but not Burkitt B-cell dependency factor roles (25). Notably, BATF and Jun family members bind cooperatively with IRF transcription factors to AP1-IRF composite DNA elements (AICE) (70), and JunB is the Jun family member predominantly expressed in LCLs (**Fig. 5A**). WT and TES2m LMP1 upregulated IRF4 mRNA abundance to a similar extent in Akata, whereas TES1m did so to a somewhat lesser extent. By contrast, TES1m and TES2m each upregulated BATF but not quite as strongly as WT LMP1 (**Fig. 5B**). Taken together with the LCL LMP1 knockout data, these results suggest that LMP1 TES1 and TES2 signaling each support expression of the host transcription factors that bind to AICE.

We next examined the contribution of LMP1 NF-κB pathways to B cell IRF4 and BATF expression. LMP1 CRISPR knockout in GM12878 LCLs or in latency III Jijoye Burkitt cells significantly reduced BATF and to IRF4 expression at the protein level, though effects on IRF4 were more subtle at this early timepoint (**Fig. S7A**). To test canonical NF-κB pathway roles in IRF4 and BATF induction, we induced LMP1 in the absence or presence of a small molecule antagonist of the kinase IKKβ. LMP1 induction of IRF4 and BATF was strongly impaired by either TES1 or TES2 mutations, and IKKβ inhibition blocked their residual induction by TES1m

and TES2m (**Fig. 5C-D**). The IKKβ inhibitor reduced BATF and IRF4 expression in GM12878 (**Fig. S7B**). Similar results were obtained in Akata cells that co-induced LMP1 with an IκBα super-repressor (IκBα-SR), in which IκBα serine 32 and 36 to alanine point mutations prevent its canonical pathway phosphorylation and proteasomal degradation (**Fig. S7C**). Furthermore, CRISPR knockout of the canonical NF-κB pathway kinase TAK1 significantly impaired IRF4 induction by WT and also TES2m LMP1 (**Fig. 5E**). Taken together, these results suggests that canonical NF-κB pathways driven by both TES1 and TES2 signaling are each important for BATF and IRF4 expression (**Fig. 5F**).

LMP1 TES1 and TES2 roles in EBV Super-Enhancer target induction

The five LMP1-activated NF-κB transcription factor subunits and four EBNAs target a set of LCL enhancers termed EBV super-enhancers (EBV SE), characterized by markedly higher and broader histone H3K27ac ChIP-seq signals than at typical LCL enhancers (**Fig. 6A**). SE are critical for cell identity and oncogenic states (71), and EBV SE are important for LCL growth and survival (72-74). Little has remained known about the extent to which individual LMP1 NF-κB pathways or NF-κB transcription factors contribute to EBV SE. To gain insights, we therefore interrogated EBV SE gene target responses to TES1 or TES2 point mutation. We first plotted EBV SE gene target responses to LMP1 CRISPR KO in GM12878. At the early timepoint of 48 hours after LMP1 editing, expression of SE targets TRAF1, PRDM1 (which encodes the transcription repressor BLIMP1) and GPR15 each significantly decreased, though most other EBV SE gene targets did not significantly change at this early timepoint (**Fig. 6B**). This data suggests that EBV SE are robust to short-term perturbations of LMP1 expression, perhaps given persistence of the established epigenetic landscape built at these key sites.

To then identify the extent to which LMP1 is sufficient to alter expression of these LCL EBV SE targets, we next visualized effects of conditional LMP1 induction in our Burkitt models. In Akata B cells, WT LMP1 induction was sufficient to significantly upregulate the abundance of the majority of EBV SE target gene mRNAs (**Fig. 6C**). This result suggests that while EBNA-2, LP, 3A and 3C also target these sites in LCL, that LMP1 can independently alter expression of most EBV SE targets, albeit not necessarily to the same extent. By contrast, Akata TES1m or TES2m induction less strongly induced most EBV SE targets (**Fig. 6D-E**). A similar pattern was observed in BL-41 cells (**Fig. S8**). Taken together, our results indicate that TES1 and TES2 likely play key joint roles in the induction of EBV SE target genes.

Discussion:

A longstanding question has remained why two LMP1 C-terminal tail domains are each necessary for lymphoblastoid B-cell immortalization. To gain insights, we performed the first systematic cross-comparison of B-cell transcriptome-wide effects of wildtype LMP1, or LMP1 point mutants abrogated for signaling by TES1 or TES2. Our analyses highlight independent, shared and antagonistic LMP1 TES1 and TES2 roles in B-cell genome-wide target gene regulation. K-means analyses of host gene responses to LMP1 WT, TES1, TES2 or DM highlighted six clusters. These included host target genes that responded more strongly to TES1 than TES2, that were similarly upregulated by either TES1 or TES2, that were downmodulated by either TES in a manner that is negatively regulated by the other, that were induced by TES2 but dampened by TES1, or that were inhibited by both TES1 and TES2 (**Fig. 7**). LMP1 B-cell target genes were further validated by cross-comparison with LCL genes that rapidly changed upon LMP1 knockout, at an early timepoint where cells remained viable. A set of LMP1-targeted LCL dependency factors were identified. We speculate that many of the observed changes occur at the transcriptional level. However, it remains possible that superimposed LMP1 effects on mRNA stability or processing could also shape the observed mRNA abundance landscape.

How independent or combined TES1 and TES2 signaling have different effects on these clusters of target genes will be important to define. With regards to Cluster 1 genes, which were induced weakly by TES2 signaling, somewhat more by TES1 signaling but more highly by WT LMP1, we speculate that TES1 and TES2 may cross-talk at the epigenetic level. For example, our results are consistent with a model in which TES1 signaling increases chromatin accessibility at these sites, including the genes encoding IFIT1 and CXCL9. Once accessible, both TES1 and TES2 signal-dependent pathways may then additively or perhaps synergistically upregulate these sites. Alternatively, TES1 signaling could be needed to dismiss a repressor, such that these sites can then be stimulated by both LMP1 domains. TES1 signaling may also activate a key positive regulator such as BCL3 (75), which then functions together with transcription factors activated by TES1 and TES2 pathways. Further studies will be required to discriminate between these and other possibilities. By contrast, Cluster 6 genes appeared to be additively repressed by TES1 and TES2 signaling. TES1 and TES2 may recruit co-repressors to these sites, may additively recruit the same repressor or may reduce chromatin accessibility.

Cluster 2 genes were similarly induced by WT LMP1, TES1m and TES2m, suggesting that signaling from either TES is sufficient to regulate their expression. While still potentially critical for EBV-driven B-cell transformation, growth and survival, this category of genes is unlikely to account for the observation that both TES1 and TES2 signaling are each necessary for B-cell immortalization by EBV. It is plausible that these genes are strongly induced by a pathway shared by TES1 and TES2, such as a canonical NF-κB pathway. Although at times referred to as an activator of non-canonical NF-κB, TES1 signaling also strongly activates canonical NF-κB (13, 15, 76), as observed in our BATF and IRF4 studies. MAP kinases activated by TES1 and by TES2 may likewise drive upregulation of this group of LMP1 targets, which were enriched for both NF-κB and MAPK signaling.

We identified a third cluster of LMP1 response genes, in which unopposed TES2 signaling caused target gene downregulation (**Fig. 7**). As Cluster 3 was enriched for metabolism genes, this observation raises the possibility that TES1 mutant EBV fails to support lymphoblastoid B-cell transformation at times following day 8 post-infection (40, 45) due to alterations in EBV-

remodeled metabolic pathways, such as glutathione metabolism or OXPHOS (77-80). It is possible that TES2 induces a repressor that targets these sites, but that TES1 signaling serves to blunt its induction. Alternatively, TES1 signaling may induce an activator that counterbalances TES2-driven repressor activity. Or, TES2 signaling may reduce chromatin accessibility at these sites in the absence of TES1. By contrast, Cluster 5 genes were upregulated by unopposed TES2 signaling, but not by WT LMP1 or unopposed TES1 signaling. TES1 signaling may instead recruit repressors or alter chromatin accessibility at these sites. Epigenetic analyses of histone repressive marks, such as ChIP studies of H3K9me3 and H3K27me3, as well as ATAC-seq studies of DNA packaging, should help to differentiate between these and other possibilities.

Although BATF was originally found to be an EBNA2 target gene (81), our studies identify that it is also targeted by LMP1. Canonical NF-κB signaling downstream of TES1 and TES2 contributed to BATF induction in Burkitt cells, where EBNA2 is not expressed, and BATF expression rapidly decreased in LCLs upon LMP1 KO. Thus, EBNA2 and LMP1/canonical NF-κB may jointly induce this critical LCL dependency factor, which has key roles in support of EBNA3A/C transcription regulation and in support of MYC (25, 82, 83). LMP1 canonical NF-κB pathways were also critical for inducing IRF4, which binds with BATF to composite AICE DNA sites and which has key roles in EBNA3C targeting to DNA sites (84) and maintenance of EBV latency (85). As EBNA3C also supports IRF4 expression (86), and as LMP1 PI3K and SRC signaling are also important for LMP1 induction of IRF4 (87, 88), our results further highlight BATF and IRF4 as major hubs of EBV oncoprotein cross-talk.

We previously used ChIP-seq to characterize the LCL NF-κB genomic binding landscape (32). Rather than identifying readily recognizable LMP1 canonical versus non-canonical NF-κB target genes, this study identified complex patterns of occupancy by the five NF-κB transcription factor subunits at LCL enhancers and promoters. However, LCL enhancers often target multiple genes, often from long distances (72), complicating cross-comparison with this study. Furthermore, concurrent LMP1 TES1 and TES2 signaling yields up to 13 distinct NF-κB transcription factor dimers in LCL nuclei (32), including dimers such as cRel:p52 that are under control of both NF-κB pathways. Conditional expression of TES1m or TES2m should yield a considerably less complex NF-κB. Therefore, a future objective will therefore be to perform NF-κB ChIP-seq in using the conditional TES1m and TES2m conditional Burkitt models reported here, as these may yield less complex patterns of NF-κB occupancy. This approach may further help to explain why LMP1 canonical and non-canonical NF-κB pathways are each critical for LCL proliferation (25).

LMP1 knockout rapidly altered expression of ~3400 LCL genes. We do not suspect that these changes were secondary to cell death, as we performed profiling on viable cells at an early timepoint post-CRISPR editing. Furthermore, conditional LMP1 inactivation caused LCL growth arrest rather than death (89), and our GSEA analysis found NF-κB signaling to be highly enriched amongst genes downregulated by LMP1 KO, suggesting on-target effects. It will be of interest to conditionally express TES1m or TES2m LMP1 concurrently with endogenous LCL LMP1 KO to gain further insights into TES1 and TES2 specific and joint roles in the lymphoblastoid B-cell context.

Our studies provide insights into TES1 and TES2 roles in regulation of B-cell EBV SE targets. Although EBV SE are highly co-occupied by all five LMP1-activated NF-κB B subunits, individual TES1 and TES2 roles in upregulation of these key LCL gene targets has remained

unstudied. Interestingly, we found that signaling by either TES1 or TES2 was sufficient to highly induce large subsets of EBV SE targets. Notably, TES2m induced a larger number of EBV SE targets, perhaps because TES1 highly induces both canonical and non-canonical pathways and therefore activates all 5 NF-κB subunits. By contrast, LMP1 KO perturbed expression of only a small number of EBV SE targets, likely because epigenetic remodeling of these sites and occupancy by EBNA and other host transcription factors allowed robustness over the short window of the experiment. An interesting future question will be to define TES1 and TES2 roles in regulation of anti-tumor immunity (90).

While we observed concordance between key aspects of RNAseq studies conducted in the Akata and BL-41 contexts, we speculate that differences may arise from distinct host genome mutation landscapes between these two human tumor derived models. For instance, tumor genome mutations alter basal signaling of key pathways, including of NF-κB. EBV+ Burkitt have higher overall mutation burdens likely driven by activation-induced cytidine deaminase (56, 57). Akata arose as an EBV+ tumor, whereas BL-41 is EBV-uninfected. Even though we used Akata cured of EBV, host genome mutations persist and shape the basal transcriptome context. Nonetheless, since EBV can infect a wide range of B-cells, including of distinct differentiation or activation states, differences between Akata and BL-41 provide insights into how LMP1 may function in differing B-cell contexts.

In summary, we identified LMP1 genome-wide B-cell targets and characterized their responses to signaling by TES1 and/or TES2. K-means analysis highlighted gene clusters with distinct expression responses to signaling by one or both LMP1 transformation essential domains. These studies highlight multiple levels by which TES1 and TES2 signaling alter LMP1 target gene expression, including by additive vs opposing roles. CRISPR KO further highlighted LCL genes that are highly sensitive to LMP1 perturbation. TES1 and TES2 roles in regulation of LCL dependency factors, including BATF and IRF4, as well as EBV SE were characterized. Collectively, these studies provide new insights into key non-redundant versus joint TES1 and TES2 roles in B-cell target gene regulation.

Acknowledgements:

This work was supported by NIH R01 CA228700 and AI164709, U01 CA275301, a Burroughs Wellcome Career Award in Medical Sciences to B.E.G, T32 T32AI007245 and an American Cancer Society Post-doctoral Fellowship to E.M.B, T32 T32AI007245 and F32 AI172329 to L.A.M.N and NIH K99 1K99DE031016 to R.G. All RNAseq and proteomics datasets will be published in the GEO omnibus GSE228158, GSE228167, and GSE228178 upon manuscript publication.

AUTHOR CONTRIBUTIONS

B.M and E.M.B performed the experiments. E.M.B, R.G and L.A.M.N performed bioinformatics analyses. B.M and B.E.G designed the experiments. B.M and B.E.G wrote the manuscript. All authors analyzed the results, read and approved the manuscript**.**

Figure Legends:

Fig. 1 RNAseq analysis of Akata B-cell responses to WT, TES1, TES2 or DM LMP1.

(A) Schematic diagram of LMP1 WT, TES1m, TES2m and DM.

(B) K-means heatmap of transcriptome responses in EBV- Akata cells to LMP1 WT, TES1m, TES2m or DM expression induced by 250 ng/ml doxycycline for 24 hours. Heatmap depicts RNAseq of host gene Log2 Fold change across n=3 independent replicates, divided into six clusters. A two-way ANOVA P value cutoff of <0.01 and >2-fold gene expression were used.

C) Heatmaps of representative Cluster 1 differentially regulated genes (top). Also shown are expression values of two representative Clusters 1 genes (lower left) and Enrichr KEGG pathway –Log 10 (adjusted p values) of significantly enriched Cluster 1 gene sets (lower right). p-values were determined by one-sided Fisher's exact test. ***p<0.001.

(D) Heatmaps of representative Cluster 2 differentially regulated genes (top). Also shown are expression values of two representative Clusters 2 genes (lower left) and Enrichr KEGG pathway –Log 10 (adjusted p values) of significantly enriched Cluster 2 gene sets (lower right). p-values were determined by one-sided Fisher's exact test. *p<0.05, **p<0.01, ***p<0.001.

(E) Heatmaps of representative Cluster 6 differentially regulated genes (top). Also shown are expression values of two representative Clusters 6 genes (lower left) and Enrichr KEGG pathway –Log 10 (adjusted p values) of significantly enriched Cluster 6 gene sets (lower right). p-values were determined by one-sided Fisher's exact test. *p<0.05, ***p<0.001.

Fig. S1 Analysis of LMP1 WT, TES1m, TES2m and DM effects in EBV-negative Akata B-cells.

(A) Immunoblot analysis of whole cell lysates (WCL) in Akata cells induced for LMP1 upon induction by 250 ng/ml doxycycline (Dox) for 24 hours as indicated. Blots are representative of n = 3 experiments.

(B) Immunoblot analysis of whole cell lysates (WCL) in BL-41 cells induced for LMP1 as indicated in (A). Blots are representative of n = 3 experiments.

(C) FACS analysis of plasma membrane (PM) ICAM-1 in Akata cells induced for LMP1 by 250 ng/ml dox for 24 hours, as indicated. For comparison, levels in GM12878 LCLs or latency I Mutu I Burkitt cells are shown.

(D) PM ICAM-1 Mean Fluorescence Intensity (MFI) + SD in Akata cells with the indicated LMP1 expression, as in (C). p-values were determined by one-sided Fisher's exact test. **p<0.001, ***p<0.0001.

(E) PM Fas MFI in Akata cells induced for LMP1 by 250ng/ml of dox for 24 hours as indicated. For comparison, levels in GM12878 LCLs or latency I Mutu I Burkitt cells are shown.

(F) PM Fas MFI + SD in Akata cells with the indicated LMP1 expression, as in (E). P-values were determined by one-sided Fisher's exact test. **p<0.001, ***p<0.0001.

(G) PM ICAM-1 MFI + SD in BL-41 cells induced for LMP1 expression by 250ng/ml dox for 24 hours, as indicated. p-values were determined by one-sided Fisher's exact test. **p<0.001, ***p<0.0001.

(H) PM ICAM-1 MFI + SD in Akata cells with the indicated LMP1 expression, as in (G). P-values were determined by one-sided Fisher's exact test. **p<0.001, ***p<0.0001.

(I) PM Fas MFI + SD in BL-41 cells induced for LMP1 expression by 250 ng/ml dox for 24 hours, as indicated. p-values were determined by one-sided Fisher's exact test. **p<0.001, ***p<0.0001.

(J) Mean Fluorescence Intensity (MFI) presented for Fas+ population in BL-41-LMP1 cells, , as in (I). p-values were determined by one-sided Fisher's exact test. **p<0.001, ***p<0.0001.

Fig. S2. RNAseq analysis of Akata B-cell responses to WT, TES1, TES2 or DM LMP1.

(A) Heatmaps of representative Cluster 3 differentially regulated genes (top). Also shown are expression values of two representative Clusters 3 genes (lower left) and Enrichr KEGG pathway –Log 10 (adjusted p values) of significantly enriched Cluster 3 gene sets (lower right). p-values were determined by one-sided Fisher's exact test. **p<0.01.

(B) Heatmaps of representative Cluster 4 differentially regulated genes (top). Also shown are expression values of two representative Clusters 4 genes (lower left) and Enrichr KEGG pathway –Log 10 (adjusted p values) of significantly enriched Cluster 4 gene sets (lower right). p-values were determined by one-sided Fisher's exact test. *p<0.05, **p<0.01, ***p<0.001.

(C) Heatmaps of representative Cluster 5 differentially regulated genes (top). Also shown are expression values of two representative Clusters 5 genes (lower left) and Enrichr KEGG pathway –Log 10 (adjusted p values) of significantly enriched Cluster 5 gene sets (lower right). p-values were determined by one-sided Fisher's exact test. *p<0.05, ***p<0.001.

Fig. S3 RNAseq analysis of BL-41 B-cell responses to WT, TES1, TES2 or DM LMP1.

(A) K-means heatmap of transcriptome responses in EBV- BL-41 cells to LMP1 WT, TES1m, TES2m or DM expression induced by 250 ng/ml doxycycline for 24 hours. Heatmap depicts RNAseq of host gene Log2 Fold change across n=3 independent replicates, divided into six clusters. A two-way ANOVA P value cutoff of <0.01 and >2-fold gene expression were used.

(B) Heatmaps of representative Cluster 1 differentially regulated genes (top). Also shown are expression values of two representative Clusters 1 genes (lower left) and Enrichr KEGG pathway –Log 10 (adjusted p values) of significantly enriched Cluster 1 gene sets (lower right). p-values were determined by one-sided Fisher's exact test. ***p<0.001.

(C) Heatmaps of representative Cluster 2 differentially regulated genes (top). Also shown are expression values of two representative Clusters 2 genes (lower left) and Enrichr KEGG pathway –Log 10 (adjusted p values) of significantly enriched Cluster 2 gene sets (lower right). p-values were determined by one-sided Fisher's exact test. ***p<0.001.

(D) Heatmaps of representative Cluster 4 differentially regulated genes (top). Also shown are expression values of two representative Clusters 4 genes (lower left) and Enrichr KEGG pathway –Log 10 (adjusted p values) of significantly enriched Cluster 4 gene sets (lower right). p-values were determined by one-sided Fisher's exact test. *p<0.05, ***p<0.001.

(E) Heatmaps of representative Cluster 6 differentially regulated genes (top). Also shown are expression values of two representative Clusters 6 genes (lower left) and Enrichr KEGG

pathway –Log 10 (adjusted p values) of significantly enriched Cluster 6 gene sets (lower right). p-values were determined by one-sided Fisher's exact test. *p<0.05, **p<0.01, ***p<0.001.

Fig. 2. Effects of LMP1 signaling on the Akata transcriptome.

(A) Volcano plot analysis of Akata RNA-seq, comparing mRNA values in cells induced for LMP1 WT for 24 hours vs. mock-induced.

(B) Enrichr KEGG pathways most highly changed in WT versus uninduced Akata, as in (A).

(C) Volcano plot analysis of Akata RNA-seq, comparing mRNA values in cells induced for LMP1 WT vs LMP1 TES1m for 24 hours.

(D) Enrichr KEGG pathways most highly changed with WT versus LMP1 TES1m expression, as in (C).

(E) Volcano plot analysis of Akata RNA-seq, comparing mRNA values in cells induced for LMP1 WT vs LMP1 TES2m for 24 hours.

(F) Enrichr KEGG pathways most highly changed with WT versus LMP1 TES2m expression, as in (E).

(G) Volcano plot analysis of Akata RNA-seq, comparing mRNA values in cells induced for LMP1 WT vs LMP1 DM for 24 hours.

(H) Enrichr KEGG pathways most highly changed with WT versus LMP1 DM expression, as in (G).

Fig. S4. Effects of LMP1 signaling on the BL-41 transcriptome.

(A) Volcano plot analysis of BL-41 RNA-seq, comparing mRNA values in cells induced for LMP1 WT for 24 hours vs. mock-induced.

(B) Enrichr KEGG pathways most highly changed in WT versus uninduced BL-41, as in (A).

(C) Volcano plot analysis of BL-41 RNA-seq, comparing mRNA values in cells induced for LMP1 WT vs LMP1 TES1m for 24 hours.

(D) Enrichr KEGG pathways most highly changed with WT versus LMP1 TES1m expression, as in (C).

(E) Volcano plot analysis of BL-41 RNA-seq, comparing mRNA values in cells induced for LMP1 WT vs LMP1 TES2m for 24 hours.

(F) Enrichr KEGG pathways most highly changed with WT versus LMP1 TES2m expression, as in (E).

(G) Volcano plot analysis of BL-41 RNA-seq, comparing mRNA values in cells induced for LMP1 WT vs LMP1 DM for 24 hours.

(H) Enrichr KEGG pathways most highly changed with WT versus LMP1 DM expression, as in (G).

Fig. 3. Cross-comparison of target gene induction by LMP signaling in Akata vs BL-41.

(A) Scatter plot analysis of fold changes in mRNA abundances in cells induced for LMP1 WT for 24 hours versus uninduced. Shown are genes differentially regulated by >1 fold.

(B) Scatter plot analysis of fold changes in mRNA abundances in cells induced for LMP1 DM for 24 hours versus uninduced. Shown are genes differentially regulated by >1 fold.

(C) Scatter plot analysis of fold changes in mRNA abundances in cells induced for LMP1 TES1m for 24 hours versus uninduced. Shown are genes differentially regulated by >1 fold.

(D) Scatter plot analysis of fold changes in mRNA abundances in cells induced for LMP1 TES2m for 24 hours versus uninduced. Shown are genes differentially regulated by >1 fold.

(E) Volcano plot analysis of Akata genes differentially regulated by LMP1 TES1m vs TES2m expression for 24 hours.

(F) Enrichr KEGG pathways most highly changed with LMP1 TES1m vs TES2m expression in Akata, as in (E).

(G) Volcano plot analysis of BL-41 genes differentially regulated by LMP1 TES1m vs TES2m expression for 24 hours.

(H) Enrichr KEGG pathways most highly changed with LMP1 TES1m vs TES2m expression in BL-41, as in (G).

Fig. S5. GSEA of a subset of pathways differentially regulated by WT vs TES mutant LMP1.

(A) GSEA analysis of oxidative phosphorylation genes in Akata (left) and BL-41 (right) expressing LMP1 as indicated for 24 hours.

(B) GSEA analysis of IFN signaling genes in Akata (left) and BL-41 (right) expressing LMP1 as indicated for 24 hours.

(C) GSEA analysis of fatty acid metabolism genes in Akata (left) and BL-41 (right) expressing LMP1 as indicated for 24 hours.

(D) GSEA analysis of peroxisome genes in Akata (left) and BL-41 (right) expressing LMP1 as indicated for 24 hours.

(E) GSEA analysis of cholesterol homeostasis genes in Akata (left) and BL-41 (right) expressing LMP1 as indicated for 24 hours.

(F) GSEA analysis of unfolded protein response genes in Akata (left) and BL-41 (right) expressing LMP1 as indicated for 24 hours.

Fig. 4 CRISPR LMP1 KO effects on GM12878 LCL target gene regulation.

(A) Immunoblot analysis of WCL from GM12878 LCLs expressing control or LMP1 targeting sgRNAs and puromycin selected for 0 vs 2 days, as indicated. Blots are representative of n = 3 experiments.

(B) K-means heatmap of transcriptome responses in Latency III GM12878 LCL expressing control or LMP1 sgRNA and puromycin selected for 48 hours, as indicated. Heatmap depicts relative row Z-scores from n=3 independent RNAseq replicates, divided into two clusters. Two-way ANOVA P value cutoff of <0.01 and >2-fold gene expression cutoffs were used.

(C) Values of two representative Clusters 1 genes. p-values were determined by one-sided Fisher's exact test. *p<0.05, **p<0.01.

(D) Values of two representative Clusters 2 genes. p-values were determined by one-sided Fisher's exact test. ***p<0.001.

(E) Enrichr KEGG pathways most highly changed with LMP1 KO.

(F) Volcano plot analysis of GM12878 genes differentially regulated by LMP1 KO, as in (B).

(G) Scatter plot analysis cross comparing mRNA abundance fold changes in LMP1 sgRNA vs control (Y-axis) versus Akata expressing LMP1 WT for 24 hours vs uninduced (x-axis). Shown are genes differentially regulated by >1 fold.

(H) Volcano plot analysis of EBV mRNA values in GM12878 expressing LMP1 vs control sgRNAs, as in (B). P-value cutoff of <0.05 and >1-fold gene expression were used.

(I) Scatter plot analysis cross comparing –Log 10 p-values of GM12878 with LMP1 vs control sgRNA (Y-axis) versus CRISPR LCL vs Burkitt cell dependency factor analysis from (25) (X-axis). Shown are genes with p<0.05 in both analyses.

(J) String analysis of genes shown in (I). Respective pathways for each gene and interaction are colored coded.

Fig. S6. CRISPR LMP1 KO effects on GM12878 LCL target gene regulation.

(A) Relative mean + SD live cell numbers from CellTitreGlo analysis of n=3 replicates of Cas9+ GM12878 LCL expressing control or LMP1 sgRNAs and puromycin selected for 0 vs 2 days.

(B) Scatter plot analysis cross comparing mRNA abundance fold changes in LMP1 sgRNA vs control (Y-axis) versus Akata expressing LMP1 TES1m for 24 hours vs uninduced (x-axis). Shown are genes differentially regulated by >1 fold.

(C) Scatter plot analysis cross comparing mRNA abundance fold changes in LMP1 sgRNA vs control (Y-axis) versus Akata expressing LMP1 TES2m for 24 hours vs uninduced (x-axis). Shown are genes differentially regulated by >1 fold.

(D) Scatter plot analysis cross comparing Log2 Fold change of GM12878 with LMP1 vs control sgRNA (Y-axis) versus CRISPR LCL vs Burkitt cell dependency factor analysis from (25) (X-axis). Shown are genes whose abundances changed by >1 fold in LMP1 KO vs control GM12878.

Fig. 5 Roles of TES1 and TES2 canonical NF-κB pathways in LCL dependency factor BATF and IRF4 induction.

(A) Schematic diagram of JUNB, BATF and IRF4 at an AP-1/IRF composite DNA site.

(B) Log2 Fold changes + SD of IRF4, BATF and JUNB mRNA abundances from n=3 RNAseq replicates of Akata expressing the indicated LMP1 construct for 24 hours, as in Fig. 1. p-values were determined by one-sided Fisher's exact test. *p<0.05, ***p<0.001.

(C) Schematic diagram of LMP1 TES1 and TES2 NF-□B signaling. TES1 and TES2 can each activate canonical NF-κB pathways.

(D) Immunoblot analysis of WCL from Akata cells induced for LMP1 expression by 250 ng/ml doxycycline for 24 hours, either without or with 1 □M IKK□ inhibitor VIII for 24 hours. Shown below are relative foldchanges + SD of IRF4 or BATF vs GAPDH load control densitometry values from n=3 replicates, with values in vehicle control treated WT LMP1 expressing cells set to 1. P-values were determined by one-sided Fisher's exact test. **p<0.001, ***p<0.0001.

(E) Immunoblot analysis of WCL from Akata cells expressing control or either of two *TAK1* targeting sgRNAs, induced for LMP1 expression by 250 ng/ml doxycycline for 24 hours. Shown below are relative foldchanges + SD of IRF4 or BATF vs GAPDH load control densitometry values from n=3 replicates, with values in sgControl/WT LMP1 expressing cells set to 1. **p<0.001, ***p<0.0001.

(F) Model of additive TES1 and TES2 effects on BATF and IRF4 induction.

Fig. S7 Roles of TES1 and TES2 canonical NF-κB pathways in BATF and IRF4 induction.

(A) Immunoblot analysis of WCL from latency III Jijoye Burkitt cells or GM12878 LCL expressing control or a *LMP1* targeting sgRNA. Shown below are relative foldchanges + SD of IRF4 or BATF vs GAPDH load control densitometry values from n=3 replicates, with values in sgControl expressing cells set to 1. P-values were determined by one-sided Fisher's exact test. **p<0.001, ***p<0.0001.

(B) Immunoblot analysis of WCL from GM12878 cells treated with vehicle control or 1 □M IKK□ inhibitor VIII for 24 hours. Shown below are relative foldchanges + SD of IRF4 or BATF vs GAPDH load control densitometry values from n=3 replicates, with values in vehicle control treated WT LMP1 expressing cells set to 1. P-values were determined by one-sided Fisher's exact test. **p<0.001, ***p<0.0001.

(C) Immunoblot analysis of WCL from Akata cells induced for the indicated LMP1 construct expression, either without or together with an IκBα super-repressor (I□B□-S.R.) that blocks canonical NF-κB signaling. Shown below are relative foldchanges + SD of IRF4 or BATF vs GAPDH load control densitometry values from n=3 replicates, with values in cells expressing WT LMP1 but not I□B□- set to 1. P-values were determined by one-sided Fisher's exact test. **p<0.001, ***p<0.0001.

Fig. 6 LMP1 TES1 and TES2 roles in EBV super-enhancer target gene regulation in GM12878 LCL and Akata B-cell.

(A) Schematic diagram of typical LCL enhancers vs super-enhancers. Super-enhancers have significantly broader and taller histone 3 lysine 27 acetyl (H3K27Ac) peaks and are bound by all five LMP1-activated NF-κB transcription factor subunits, EBNA-2, LP, 3A, and 3C.

(B) Volcano plot of mRNA values in GM12878 expressing LMP1 vs control sgRNAs as in **Fig. 4F**. Genes targeted by EBV super-enhancers (SE) are highlighted by red circles, whereas other

LCL genes are indicated by blue circles. P value cutoff of <0.05 and >1-fold gene expression were used.

(C) Volcano plot analysis of Akata RNA-seq, comparing mRNA values in cells induced for LMP1 WT vs. mock-induced for 24 hours, as in **Fig. 2A**. SE targeted genes highlighted by red circles and other B-cell genes indicated by blue circles. P value cutoff of <0.05 and >1-fold gene expression were used.

(D) Volcano plot analysis of Akata RNA-seq, comparing mRNA values in cells induced for LMP1 TES1m vs. mock-induced for 24 hours, as in **Fig. 2C**. SE targeted genes highlighted by red circles and other B-cell genes indicated by blue circles. P value cutoff of <0.05 and >1-fold gene expression were used.

(E) Volcano plot analysis of Akata RNA-seq, comparing mRNA values in cells induced for LMP1 TES2m for 24 hours vs. mock-induced, as in **Fig. 2E.** SE targeted genes highlighted by red circles and other B-cell genes indicated by blue circles. P value cutoff of <0.05 and >1-fold gene expression were used.

Fig. S8 LMP1 TES1 and TES2 roles in EBV super-enhancer target gene regulation in BL-41 B-cell.

(A) Volcano plot analysis of BL-41 RNA-seq, comparing mRNA values in cells induced for LMP1 WT vs. mock-induced for 24 hours as in **Fig. S4A**. SE targeted genes highlighted by red circles and other B-cell genes indicated by blue circles. P value cutoff of <0.05 and >1-fold gene expression were used.

(B) Volcano plot analysis of BL-41 RNA-seq, comparing mRNA values in cells induced for LMP1 TES1m vs. mock-induced for 24 hours as in **Fig. S4C**. SE targeted genes highlighted by red circles and other B-cell genes indicated by blue circles. P value cutoff of <0.05 and >1-fold gene expression were used.

(C) Volcano plot analysis of BL-41 RNA-seq, comparing mRNA values in cells induced for LMP1 TES2m vs. mock-induced for 24 hours as in **Fig. S4E**. SE targeted genes highlighted by red circles and other B-cell genes indicated by blue circles. P value cutoff of <0.05 and >1-fold gene expression were used.

Fig. 7 Model highlighting different modes of LMP1 TES1 and TES2 cross-talk in B-cell target gene regulation.

Materials and Methods

Cell lines, culture, and vectors. HEK293T cells were purchased from ATCC and cultured in Dulbecco's modified Eagle medium (DMEM, Gibco) with 10% fetal bovine serum (FBS, Gibco). EBV-negative Akata and BL-41 cells were obtained from Elliott Kieff; GM12878 were purchased from Coriell. Mutu I was obtained from Jeff Sample and Jijoye was purchased from ATCC. All B-cell lines stably expressed *Streptococcus pyogenes* Cas9 and were grown in Roswell Park Memorial Institute (RPMI) 1640 (Life Technologies) with 10% fetal bovine serum (Gibco) and penicillin-streptomycin in a humidified chamber with 5% carbon dioxide. LMP1 wildtype, TES1 alanine point mutant 204PQQAT208 -> AQAAT, TES2 384YYD386->ID mutant and double mutant LMP1 with both AXAXT and ID mutations were cloned into the pLIX-402 vector. pLIX-402 uses a TET-On TRE promoter to drive transgene expression and a C-terminal HA-tag fusion. Lentivirus vectors were used to establish stable Cas9+/EBV- Akata and Cas9+/EBV- BL-41 Burkitt cells. Cell lines were then maintained with 0.5 µg/mL puromycin or 25 µg/mL hygromycin. For LMP1 inducible expression studies, 0.5X10^6 cells/ml were plated on Day-1 in 2ml of fresh RPMI in a 12-well plate. Cell were treated with 250ng/ml doxycycline (Sigma #D9891) for 24 hours on Day 0 and were collected for downstream analyses on Day 1. The Iκβα Super-repressor (SR) lacking residues 1-67 has previously been reported (27).

Antibodies and Reagents. Cell Signaling Technology (CST) TRAF1 (#4715, Rabbit mAb), p105/50 (#3035, Rabbit mAb), RelA (#8242, Rabbit mAb), phospho-RelA (Ser536) (3033, Rabbit mAb), RelB (#4922, Rabbit mAb), cRel (#4727, Rabbit mAb), IκBα (#9247, Mouse mAb), IRF4 (#4964, Rabbit mAb), TAK1 (#4505, Rabbit mAb), V5 (#13202, Rabbit mAb), HRP-linked anti-mouse IgG(7076), HRP-linked anti-rabbit IgG (#7074) were used in this study at 1:1000 dilution. p100/52 (EMD Millipore #05-361, Mouse mAb, 1:1000), GAPDH (EMD Millipore #MAB374, Mouse mAb, 1:500) was used. S12 mouse monoclonal antibody against LMP1 was purified from hybridoma supernatant (91). The IKKβ inhibitor IKK-2 inhibitor VIII (ApexBio, #A3485), puromycin dihydrochloride (Thermo Fisher #A1113803), and hygromycin B (Millipore #400052).

Growth Curve Analysis: For growth curve analysis, cells were counted and then normalized to the same starting concentration, using the CellTiterGlo (CTG) luciferase assay (Promega, Cat#G7570). Live cell numbers were quantitated at each timepoint by CTG measurements, and values were corrected for tissue culture passage. Fold change of live cell number at each timepoint was calculated as a ratio of the value divided by the input value.

CRISPR/Cas9 editing. B-cell lines with stable Cas9 expression were established as described previously (62). Briefly, HEK293T cells were plated at a density of 300,000 cells per well in 2 mL DMEM supplemented with 10% FBS on Day -1. The following day (Day 0) plated cells were transfected with the TransIT-LT1 Transfection Reagent (Mirus #2306), according to the manufacturer's protocol. Transfection media was replaced by RPMI 16 hours later (Day 1). B-cells were plated at 1.2X 10^6 density in a 6-well plate on Day 1. Lentivirus collected on Day 2 were added to the B-cells for spinoculation at 2000rpm for 2 hours at 37C and 4µg/ml of polybrene. Spinoculated cells were placed in in a humidified chamber with 5% carbon dioxide for 6 hours, then pelleted and resuspended in fresh RPMI/FBS. 48 hours post-transduction, puromycin 3 µg/ml or 200 µg/ml hygromycin was added to select transduced cells. Broad Institute pXPR-515 control sgRNA (targes a non-coding intergenic region), Avana or Brunello library sgRNAs, as listed in Table 1, were cloned into lentiGuide-Puro (Addgene, catalog #52963) or pLenti SpBsmBI sgRNA Hygro (Addgene, catalog #62205).

RNAseq. Total RNA was isolated using RNeasy mini kit (Qiagen #74106) with in-column genomic DNA digestion step according to the manufacturer's protocol. To construct indexed libraries, 1 µg of total RNA was used for polyA mRNA selection using NEBNext Poly(A) mRNA Magnetic Isolation Module (Cat#E7490S), and library preparation with NEBNext Ultra RNA Library Prep

with Sample Purification Beads (Cat#E7765S). Each experimental treatment was performed in biological triplicate. Libraries were multi-indexed (NEB 7335L and E7500S), pooled and sequenced on an Illumina NextSeq 500 sequencer using single 75 bp read length. Adaptor-trimmed Illumina reads for each individual library were mapped back to the human GRCh37.83 transcriptome assembly using STAR2.5.2b (92). FeatureCounts was used to estimate the number of reads mapped to each contig (93). Only transcripts with at least 5 cumulative mapping counts were used in this analysis. DESeq2 was used to evaluate differential expression (DE) (94). DESeq2 uses a negative binomial distribution to account for overdispersion in transcriptome data sets. It is conservative and uses a heuristic approach to detect outliers while avoiding false positives. Each DE analysis was composed of a pairwise comparison between experimental group and the control group. Differentially expressed genes were identified after a correction for false discovery rate (FDR). For more stringent analyses, we set the cutoff for truly differentially expressed genes as adjusted p value (FDR corrected) < 0.05 and absolute fold change > 1.5. DE genes meeting this cutoff were selected and subject to downstream bioinformatics and functional analyses, including clustering, data visualization, GO annotation and pathway analysis. DE genes were also subjected to Enrichr analysis (https://maayanlab.cloud/Enrichr/) for pathway analysis and GO annotations. We also performed gene list-based gene set enrichment analysis on the DE gene subset leading to pathway enrichment analysis of the ranked gene list using GSEA computational software (95, 96). Venn diagrams were generated using a web-based application for the same (https://bioinformatics.psb.ugent.be/webtools/Venn/). Heatmaps were generated by feeding the Variance-Stabilizing Transformed values of selected DE genes from DESeq2 into Morpheus (https://software.broadinstitute.org/morpheus/).

Immunoblot Analysis. Cells were lysed in Laemelli buffer (0.2M Tris-HCL, 0.4 M Dithiothreitol, 277mM SDS, 6mM Bromophenol blue and 10% glycerol v/v) and sonicated at 4℃ for five seconds using a probe sonicator at 20% amplitude and boiled at 95℃ for eight minutes. The whole cell lysates were resolved by 12% or 15% SDS-PAGE, transferred to nitrocellulose filters at 100V at 4℃ for 1.5 hour, blocked with 5% non-fat dried milk in 1X TBST for 30 min at room-temperature, and then probed with the indicated primary antibodies (diluted in 1x TBS-T with 0.02% sodium azide at recommended manufacturer concentrations) overnight at 4℃ on a rotating platform. Blots were washed three times in TBST for ten minutes each, and then probed with horse-radish peroxidase (HRP)-conjugated secondary antibodies, at a dilution of 1:3000 in 1X TBST with 5% non-fat dried milk. Blots were then washed three times in TBST for ten minutes each, developed by ECL chemiluminescent substrate (Thermo Scientific, #34578) and imaged on Li-COR Odyssey workstation.

Flow cytometry analysis. FACS was performed using a FACSCalibur instrument (BD). For ICAM-1 and FAS detection, cells were washed in PBS w/2%FBS, then stained on ice for 30 min with BioLegend PE-conjugated anti-CD54/ICAM-1 and APC-conjugated anti-CD95/Fas antibody, washed three times with PBS with 2%FBS and analyzed by FACS.

Bioinformatic analysis and Software: All the growth curves and column charts were made with GraphPad Prism v.9. FACS data was analyzed by FlowJo V10.

Table 1. sgRNAs used in this study.

Guide No.	Gene Target	sgRNA Sequence (5’ -> 3’)
#1	Control	TTGACCTTTACCGTCCCGCG

#1	LMP1	TCTATCTACAACAAAACTGG
#1	TAK1	CACCGGCTTACTGCTGGTTGCAGGG
#2	TAK1	CACCGCGCAATGAGTTGGTGTTTAC

References

1. Gewurz BE, Longnecker, R. & Cohen, J.L. . 2021. Fields Virology, 7 ed, vol 2. Wolters Kluwer.
2. Stunz LL, Bishop GA. 2014. Latent membrane protein 1 and the B lymphocyte-a complex relationship. Crit Rev Immunol 34:177-98.
3. Wang LW, Jiang S, Gewurz BE. 2017. Epstein-Barr Virus LMP1-Mediated Oncogenicity. J Virol 91.
4. Kieser A, Sterz KR. 2015. The Latent Membrane Protein 1 (LMP1). Curr Top Microbiol Immunol 391:119-49.
5. Wang L, Ning S. 2021. New Look of EBV LMP1 Signaling Landscape. Cancers (Basel) 13.
6. Fish K, Comoglio F, Shaffer AL, 3rd, Ji Y, Pan KT, Scheich S, Oellerich A, Doebele C, Ikeda M, Schaller SJ, Nguyen H, Muppidi J, Wright GW, Urlaub H, Serve H, Staudt LM, Longnecker R, Oellerich T. 2020. Rewiring of B cell receptor signaling by Epstein-Barr virus LMP2A. Proc Natl Acad Sci U S A 117:26318-26327.
7. Weniger MA, Küppers R. 2021. Molecular biology of Hodgkin lymphoma. Leukemia 35:968-981.
8. Soni V, Cahir-McFarland E, Kieff E. 2007. LMP1 TRAFficking activates growth and survival pathways. Adv Exp Med Biol 597:173-87.
9. Kaykas A, Worringer K, Sugden B. 2002. LMP-1's transmembrane domains encode multiple functions required for LMP-1's efficient signaling. J Virol 76:11551-60.
10. Rastelli J, Hömig-Hölzel C, Seagal J, Müller W, Hermann AC, Rajewsky K, Zimber-Strobl U. 2008. LMP1 signaling can replace CD40 signaling in B cells in vivo and has unique features of inducing class-switch recombination to IgG1. Blood 111:1448-55.
11. Meckes DG, Jr., Menaker NF, Raab-Traub N. 2013. Epstein-Barr virus LMP1 modulates lipid raft microdomains and the vimentin cytoskeleton for signal transduction and transformation. J Virol 87:1301-11.
12. Shair KH, Bendt KM, Edwards RH, Bedford EC, Nielsen JN, Raab-Traub N. 2007. EBV latent membrane protein 1 activates Akt, NFkappaB, and Stat3 in B cell lymphomas. PLoS Pathog 3:e166.
13. Greenfeld H, Takasaki K, Walsh MJ, Ersing I, Bernhardt K, Ma Y, Fu B, Ashbaugh CW, Cabo J, Mollo SB, Zhou H, Li S, Gewurz BE. 2015. TRAF1 Coordinates Polyubiquitin Signaling to Enhance Epstein-Barr Virus LMP1-Mediated Growth and Survival Pathway Activation. PLoS Pathog 11:e1004890.
14. Kung CP, Meckes DG, Jr., Raab-Traub N. 2011. Epstein-Barr virus LMP1 activates EGFR, STAT3, and ERK through effects on PKCdelta. J Virol 85:4399-408.
15. Mainou BA, Everly DN, Jr., Raab-Traub N. 2007. Unique signaling properties of CTAR1 in LMP1-mediated transformation. J Virol 81:9680-92.
16. Zhang L, Wu L, Hong K, Pagano JS. 2001. Intracellular signaling molecules activated by Epstein-Barr virus for induction of interferon regulatory factor 7. J Virol 75:12393-401.
17. Floettmann JE, Rowe M. 1997. Epstein-Barr virus latent membrane protein-1 (LMP1) C-terminus activation region 2 (CTAR2) maps to the far C-terminus and requires oligomerisation for NF-kappaB activation. Oncogene 15:1851-8.
18. Huen DS, Henderson SA, Croom-Carter D, Rowe M. 1995. The Epstein-Barr virus latent membrane protein-1 (LMP1) mediates activation of NF-kappa B and cell surface phenotype via two effector regions in its carboxy-terminal cytoplasmic domain. Oncogene 10:549-60.
19. Voigt S, Sterz KR, Giehler F, Mohr AW, Wilson JB, Moosmann A, Kieser A. 2020. A central role of IKK2 and TPL2 in JNK activation and viral B-cell transformation. Nat Commun 11:685.

20. Shkoda A, Town JA, Griese J, Romio M, Sarioglu H, Knöfel T, Giehler F, Kieser A. 2012. The germinal center kinase TNIK is required for canonical NF-κB and JNK signaling in B-cells by the EBV oncoprotein LMP1 and the CD40 receptor. PLoS Biol 10:e1001376.
21. Schultheiss U, Püschner S, Kremmer E, Mak TW, Engelmann H, Hammerschmidt W, Kieser A. 2001. TRAF6 is a critical mediator of signal transduction by the viral oncogene latent membrane protein 1. Embo j 20:5678-91.
22. Arcipowski KM, Stunz LL, Bishop GA. 2014. TRAF6 is a critical regulator of LMP1 functions in vivo. Int Immunol 26:149-58.
23. Arcipowski KM, Stunz LL, Graham JP, Kraus ZJ, Vanden Bush TJ, Bishop GA. 2011. Molecular mechanisms of TNFR-associated factor 6 (TRAF6) utilization by the oncogenic viral mimic of CD40, latent membrane protein 1 (LMP1). J Biol Chem 286:9948-55.
24. Wang L, Howell MEA, Sparks-Wallace A, Zhao J, Hensley CR, Nicksic CA, Horne SR, Mohr KB, Moorman JP, Yao ZQ, Ning S. 2021. The Ubiquitin Sensor and Adaptor Protein p62 Mediates Signal Transduction of a Viral Oncogenic Pathway. mBio 12:e0109721.
25. Ma Y, Walsh MJ, Bernhardt K, Ashbaugh CW, Trudeau SJ, Ashbaugh IY, Jiang S, Jiang C, Zhao B, Root DE, Doench JG, Gewurz BE. 2017. CRISPR/Cas9 Screens Reveal Epstein-Barr Virus-Transformed B Cell Host Dependency Factors. Cell Host Microbe 21:580-591.e7.
26. Gewurz BE, Towfic F, Mar JC, Shinners NP, Takasaki K, Zhao B, Cahir-McFarland ED, Quackenbush J, Xavier RJ, Kieff E. 2012. Genome-wide siRNA screen for mediators of NF-κB activation. Proc Natl Acad Sci U S A 109:2467-72.
27. Gewurz BE, Mar JC, Padi M, Zhao B, Shinners NP, Takasaki K, Bedoya E, Zou JY, Cahir-McFarland E, Quackenbush J, Kieff E. 2011. Canonical NF-kappaB activation is essential for Epstein-Barr virus latent membrane protein 1 TES2/CTAR2 gene regulation. J Virol 85:6764-73.
28. Bentz GL, Moss CR, 2nd, Whitehurst CB, Moody CA, Pagano JS. 2015. LMP1-Induced Sumoylation Influences the Maintenance of Epstein-Barr Virus Latency through KAP1. J Virol 89:7465-77.
29. Selby TL, Biel N, Varn M, Patel S, Patel A, Hilding L, Ray A, Ross T, Cramblet WT, Moss CR, Lowrey AJ, Bentz GL. 2019. The Epstein-Barr Virus Oncoprotein, LMP1, Regulates the Function of SENP2, a SUMO-protease. Sci Rep 9:9523.
30. Gires O, Kohlhuber F, Kilger E, Baumann M, Kieser A, Kaiser C, Zeidler R, Scheffer B, Ueffing M, Hammerschmidt W. 1999. Latent membrane protein 1 of Epstein-Barr virus interacts with JAK3 and activates STAT proteins. Embo j 18:3064-73.
31. Izumi KM, Cahir McFarland ED, Riley EA, Rizzo D, Chen Y, Kieff E. 1999. The residues between the two transformation effector sites of Epstein-Barr virus latent membrane protein 1 are not critical for B-lymphocyte growth transformation. J Virol 73:9908-16.
32. Zhao B, Barrera LA, Ersing I, Willox B, Schmidt SC, Greenfeld H, Zhou H, Mollo SB, Shi TT, Takasaki K, Jiang S, Cahir-McFarland E, Kellis M, Bulyk ML, Kieff E, Gewurz BE. 2014. The NF-κB genomic landscape in lymphoblastoid B cells. Cell Rep 8:1595-606.
33. Wang D, Liebowitz D, Kieff E. 1985. An EBV membrane protein expressed in immortalized lymphocytes transforms established rodent cells. Cell 43:831-40.
34. Baichwal VR, Sugden B. 1988. Transformation of Balb 3T3 cells by the BNLF-1 gene of Epstein-Barr virus. Oncogene 2:461-7.
35. Moorthy RK, Thorley-Lawson DA. 1993. All three domains of the Epstein-Barr virus-encoded latent membrane protein LMP-1 are required for transformation of rat-1 fibroblasts. J Virol 67:1638-46.
36. Minamitani T, Ma Y, Zhou H, Kida H, Tsai CY, Obana M, Okuzaki D, Fujio Y, Kumanogoh A, Zhao B, Kikutani H, Kieff E, Gewurz BE, Yasui T. 2017. Mouse model of

Epstein-Barr virus LMP1- and LMP2A-driven germinal center B-cell lymphoproliferative disease. Proc Natl Acad Sci U S A 114:4751-4756.

37. Wirtz T, Weber T, Kracker S, Sommermann T, Rajewsky K, Yasuda T. 2016. Mouse model for acute Epstein-Barr virus infection. Proc Natl Acad Sci U S A 113:13821-13826.

38. Zhang B, Kracker S, Yasuda T, Casola S, Vanneman M, Hömig-Hölzel C, Wang Z, Derudder E, Li S, Chakraborty T, Cotter SE, Koyama S, Currie T, Freeman GJ, Kutok JL, Rodig SJ, Dranoff G, Rajewsky K. 2012. Immune surveillance and therapy of lymphomas driven by Epstein-Barr virus protein LMP1 in a mouse model. Cell 148:739-51.

39. Thornburg NJ, Kulwichit W, Edwards RH, Shair KH, Bendt KM, Raab-Traub N. 2006. LMP1 signaling and activation of NF-kappaB in LMP1 transgenic mice. Oncogene 25:288-97.

40. Pich D, Mrozek-Gorska P, Bouvet M, Sugimoto A, Akidil E, Grundhoff A, Hamperl S, Ling PD, Hammerschmidt W. 2019. First Days in the Life of Naive Human B Lymphocytes Infected with Epstein-Barr Virus. mBio 10.

41. Kaye KM, Izumi KM, Kieff E. 1993. Epstein-Barr virus latent membrane protein 1 is essential for B-lymphocyte growth transformation. Proc Natl Acad Sci U S A 90:9150-4.

42. Dirmeier U, Neuhierl B, Kilger E, Reisbach G, Sandberg ML, Hammerschmidt W. 2003. Latent membrane protein 1 is critical for efficient growth transformation of human B cells by epstein-barr virus. Cancer Res 63:2982-9.

43. Cohen JI, Wang F, Kieff E. 1991. Epstein-Barr virus nuclear protein 2 mutations define essential domains for transformation and transactivation. J Virol 65:2545-54.

44. Kaye KM, Izumi KM, Mosialos G, Kieff E. 1995. The Epstein-Barr virus LMP1 cytoplasmic carboxy terminus is essential for B-lymphocyte transformation; fibroblast cocultivation complements a critical function within the terminal 155 residues. J Virol 69:675-83.

45. Izumi KM, Kaye KM, Kieff ED. 1997. The Epstein-Barr virus LMP1 amino acid sequence that engages tumor necrosis factor receptor associated factors is critical for primary B lymphocyte growth transformation. Proc Natl Acad Sci U S A 94:1447-52.

46. Devergne O, Cahir McFarland ED, Mosialos G, Izumi KM, Ware CF, Kieff E. 1998. Role of the TRAF binding site and NF-kappaB activation in Epstein-Barr virus latent membrane protein 1-induced cell gene expression. J Virol 72:7900-8.

47. Izumi KM, Kieff ED. 1997. The Epstein-Barr virus oncogene product latent membrane protein 1 engages the tumor necrosis factor receptor-associated death domain protein to mediate B lymphocyte growth transformation and activate NF-kappaB. Proc Natl Acad Sci U S A 94:12592-7.

48. Lee DY, Sugden B. 2008. The LMP1 oncogene of EBV activates PERK and the unfolded protein response to drive its own synthesis. Blood 111:2280-9.

49. Bentz GL, Whitehurst CB, Pagano JS. 2011. Epstein-Barr virus latent membrane protein 1 (LMP1) C-terminal-activating region 3 contributes to LMP1-mediated cellular migration via its interaction with Ubc9. J Virol 85:10144-53.

50. Shimizu N, Tanabe-Tochikura A, Kuroiwa Y, Takada K. 1994. Isolation of Epstein-Barr virus (EBV)-negative cell clones from the EBV-positive Burkitt's lymphoma (BL) line Akata: malignant phenotypes of BL cells are dependent on EBV. J Virol 68:6069-73.

51. Song YJ, Izumi KM, Shinners NP, Gewurz BE, Kieff E. 2008. IRF7 activation by Epstein-Barr virus latent membrane protein 1 requires localization at activation sites and TRAF6, but not TRAF2 or TRAF3. Proc Natl Acad Sci U S A 105:18448-53.

52. Huye LE, Ning S, Kelliher M, Pagano JS. 2007. Interferon regulatory factor 7 is activated by a viral oncoprotein through RIP-dependent ubiquitination. Mol Cell Biol 27:2910-8.

53. Ning S, Hahn AM, Huye LE, Pagano JS. 2003. Interferon regulatory factor 7 regulates expression of Epstein-Barr virus latent membrane protein 1: a regulatory circuit. J Virol 77:9359-68.
54. Ning S, Pagano JS. 2010. The A20 deubiquitinase activity negatively regulates LMP1 activation of IRF7. J Virol 84:6130-8.
55. Lenoir GM, Vuillaume M, Bonnardel C. 1985. The use of lymphomatous and lymphoblastoid cell lines in the study of Burkitt's lymphoma. IARC Sci Publ:309-18.
56. Thomas N, Dreval K, Gerhard DS, Hilton LK, Abramson JS, Ambinder RF, Barta S, Bartlett NL, Bethony J, Bhatia K, Bowen J, Bryan AC, Cesarman E, Casper C, Chadburn A, Cruz M, Dittmer DP, Dyer MA, Farinha P, Gastier-Foster JM, Gerrie AS, Grande BM, Greiner T, Griner NB, Gross TG, Harris NL, Irvin JD, Jaffe ES, Henry D, Huppi R, Leal FE, Lee MS, Martin JP, Martin MR, Mbulaiteye SM, Mitsuyasu R, Morris V, Mullighan CG, Mungall AJ, Mungall K, Mutyaba I, Nokta M, Namirembe C, Noy A, Ogwang MD, Omoding A, Orem J, Ott G, Petrello H, Pittaluga S, et al. 2023. Genetic subgroups inform on pathobiology in adult and pediatric Burkitt lymphoma. Blood 141:904-916.
57. Grande BM, Gerhard DS, Jiang A, Griner NB, Abramson JS, Alexander TB, Allen H, Ayers LW, Bethony JM, Bhatia K, Bowen J, Casper C, Choi JK, Culibrk L, Davidsen TM, Dyer MA, Gastier-Foster JM, Gesuwan P, Greiner TC, Gross TG, Hanf B, Harris NL, He Y, Irvin JD, Jaffe ES, Jones SJM, Kerchan P, Knoetze N, Leal FE, Lichtenberg TM, Ma Y, Martin JP, Martin MR, Mbulaiteye SM, Mullighan CG, Mungall AJ, Namirembe C, Novik K, Noy A, Ogwang MD, Omoding A, Orem J, Reynolds SJ, Rushton CK, Sandlund JT, Schmitz R, Taylor C, Wilson WH, Wright GW, Zhao EY, et al. 2019. Genome-wide discovery of somatic coding and noncoding mutations in pediatric endemic and sporadic Burkitt lymphoma. Blood 133:1313-1324.
58. Guo R, Zhang Y, Teng M, Jiang C, Schineller M, Zhao B, Doench JG, O'Reilly RJ, Cesarman E, Giulino-Roth L, Gewurz BE. 2020. DNA methylation enzymes and PRC1 restrict B-cell Epstein-Barr virus oncoprotein expression. Nat Microbiol 5:1051-1063.
59. Wang F, Gregory C, Sample C, Rowe M, Liebowitz D, Murray R, Rickinson A, Kieff E. 1990. Epstein-Barr virus latent membrane protein (LMP1) and nuclear proteins 2 and 3C are effectors of phenotypic changes in B lymphocytes: EBNA-2 and LMP1 cooperatively induce CD23. J Virol 64:2309-18.
60. Gregory CD, Rowe M, Rickinson AB. 1990. Different Epstein-Barr virus-B cell interactions in phenotypically distinct clones of a Burkitt's lymphoma cell line. J Gen Virol 71 (Pt 7):1481-95.
61. Jin J, Hu H, Li HS, Yu J, Xiao Y, Brittain GC, Zou Q, Cheng X, Mallette FA, Watowich SS, Sun SC. 2014. Noncanonical NF-κB pathway controls the production of type I interferons in antiviral innate immunity. Immunity 40:342-54.
62. Jiang S, Wang LW, Walsh MJ, Trudeau SJ, Gerdt C, Zhao B, Gewurz BE. 2018. CRISPR/Cas9-Mediated Genome Editing in Epstein-Barr Virus-Transformed Lymphoblastoid B-Cell Lines. Curr Protoc Mol Biol 121:31.12.1-31.12.23.
63. DeKroon RM, Gunawardena HP, Edwards R, Raab-Traub N. 2018. Global Proteomic Changes Induced by the Epstein-Barr Virus Oncoproteins Latent Membrane Protein 1 and 2A. mBio 9.
64. Devergne O, Hatzivassiliou E, Izumi KM, Kaye KM, Kleijnen MF, Kieff E, Mosialos G. 1996. Association of TRAF1, TRAF2, and TRAF3 with an Epstein-Barr virus LMP1 domain important for B-lymphocyte transformation: role in NF-kappaB activation. Mol Cell Biol 16:7098-108.
65. Cahir-McFarland ED, Carter K, Rosenwald A, Giltnane JM, Henrickson SE, Staudt LM, Kieff E. 2004. Role of NF-kappa B in cell survival and transcription of latent membrane protein 1-expressing or Epstein-Barr virus latency III-infected cells. J Virol 78:4108-19.

66. Shair KH, Raab-Traub N. 2012. Transcriptome changes induced by Epstein-Barr virus LMP1 and LMP2A in transgenic lymphocytes and lymphoma. mBio 3.
67. Faumont N, Durand-Panteix S, Schlee M, Grömminger S, Schuhmacher M, Hölzel M, Laux G, Mailhammer R, Rosenwald A, Staudt LM, Bornkamm GW, Feuillard J. 2009. c-Myc and Rel/NF-kappaB are the two master transcriptional systems activated in the latency III program of Epstein-Barr virus-immortalized B cells. J Virol 83:5014-27.
68. Demetriades C, Mosialos G. 2009. The LMP1 promoter can be transactivated directly by NF-kappaB. J Virol 83:5269-77.
69. Johansson P, Jansson A, Rüetschi U, Rymo L. 2009. Nuclear factor-kappaB binds to the Epstein-Barr Virus LMP1 promoter and upregulates its expression. J Virol 83:1393-401.
70. Glasmacher E, Agrawal S, Chang AB, Murphy TL, Zeng W, Vander Lugt B, Khan AA, Ciofani M, Spooner CJ, Rutz S, Hackney J, Nurieva R, Escalante CR, Ouyang W, Littman DR, Murphy KM, Singh H. 2012. A genomic regulatory element that directs assembly and function of immune-specific AP-1-IRF complexes. Science 338:975-80.
71. Hnisz D, Abraham BJ, Lee TI, Lau A, Saint-André V, Sigova AA, Hoke HA, Young RA. 2013. Super-enhancers in the control of cell identity and disease. Cell 155:934-47.
72. Jiang S, Zhou H, Liang J, Gerdt C, Wang C, Ke L, Schmidt SCS, Narita Y, Ma Y, Wang S, Colson T, Gewurz B, Li G, Kieff E, Zhao B. 2017. The Epstein-Barr Virus Regulome in Lymphoblastoid Cells. Cell Host Microbe 22:561-573.e4.
73. Zhou H, Schmidt SC, Jiang S, Willox B, Bernhardt K, Liang J, Johannsen EC, Kharchenko P, Gewurz BE, Kieff E, Zhao B. 2015. Epstein-Barr virus oncoprotein super-enhancers control B cell growth. Cell Host Microbe 17:205-16.
74. Yan B, Wang C, Chakravorty S, Zhang Z, Kadadi SD, Zhuang Y, Sirit I, Hu Y, Jung M, Sahoo SS, Wang L, Shao K, Anderson NL, Trujillo-Ochoa JL, Briggs SD, Liu X, Olson MR, Afzali B, Zhao B, Kazemian M. 2023. A comprehensive single cell data analysis of lymphoblastoid cells reveals the role of super-enhancers in maintaining EBV latency. J Med Virol 95:e28362.
75. Edwards RH, Marquitz AR, Raab-Traub N. 2015. Changes in expression induced by Epstein-Barr Virus LMP1-CTAR1: potential role of bcl3. mBio 6.
76. Kung CP, Raab-Traub N. 2010. Epstein-Barr virus latent membrane protein 1 modulates distinctive NF- kappaB pathways through C-terminus-activating region 1 to regulate epidermal growth factor receptor expression. J Virol 84:6605-14.
77. Burton EM, Voyer J, Gewurz BE. 2022. Epstein-Barr virus latency programs dynamically sensitize B cells to ferroptosis. Proc Natl Acad Sci U S A 119:e2118300119.
78. Wang LW, Shen H, Nobre L, Ersing I, Paulo JA, Trudeau S, Wang Z, Smith NA, Ma Y, Reinstadler B, Nomburg J, Sommermann T, Cahir-McFarland E, Gygi SP, Mootha VK, Weekes MP, Gewurz BE. 2019. Epstein-Barr-Virus-Induced One-Carbon Metabolism Drives B Cell Transformation. Cell Metab 30:539-555.e11.
79. Guo R, Liang JH, Zhang Y, Lutchenkov M, Li Z, Wang Y, Trujillo-Alonso V, Puri R, Giulino-Roth L, Gewurz BE. 2022. Methionine metabolism controls the B cell EBV epigenome and viral latency. Cell Metab 34:1280-1297.e9.
80. Bonglack EN, Messinger JE, Cable JM, Ch'ng J, Parnell KM, Reinoso-Vizcaíno NM, Barry AP, Russell VS, Dave SS, Christofk HR, Luftig MA. 2021. Monocarboxylate transporter antagonism reveals metabolic vulnerabilities of viral-driven lymphomas. Proc Natl Acad Sci U S A 118.
81. Johansen LM, Deppmann CD, Erickson KD, Coffin WF, 3rd, Thornton TM, Humphrey SE, Martin JM, Taparowsky EJ. 2003. EBNA2 and activated Notch induce expression of BATF. J Virol 77:6029-40.
82. Schmidt SC, Jiang S, Zhou H, Willox B, Holthaus AM, Kharchenko PV, Johannsen EC, Kieff E, Zhao B. 2015. Epstein-Barr virus nuclear antigen 3A partially coincides with

EBNA3C genome-wide and is tethered to DNA through BATF complexes. Proc Natl Acad Sci U S A 112:554-9.

83. Jiang S, Willox B, Zhou H, Holthaus AM, Wang A, Shi TT, Maruo S, Kharchenko PV, Johannsen EC, Kieff E, Zhao B. 2014. Epstein-Barr virus nuclear antigen 3C binds to BATF/IRF4 or SPI1/IRF4 composite sites and recruits Sin3A to repress CDKN2A. Proc Natl Acad Sci U S A 111:421-6.

84. Wang A, Welch R, Zhao B, Ta T, Keleş S, Johannsen E. 2015. Epstein-Barr Virus Nuclear Antigen 3 (EBNA3) Proteins Regulate EBNA2 Binding to Distinct RBPJ Genomic Sites. J Virol 90:2906-19.

85. Bristol JA, Brand J, Ohashi M, Eichelberg MR, Casco A, Nelson SE, Hayes M, Romero-Masters JC, Baiu DC, Gumperz JE, Johannsen EC, Dinh HQ, Kenney SC. 2022. Reduced IRF4 expression promotes lytic phenotype in Type 2 EBV-infected B cells. PLoS Pathog 18:e1010453.

86. Banerjee S, Lu J, Cai Q, Saha A, Jha HC, Dzeng RK, Robertson ES. 2013. The EBV Latent Antigen 3C Inhibits Apoptosis through Targeted Regulation of Interferon Regulatory Factors 4 and 8. PLoS Pathog 9:e1003314.

87. Wang L, Ren J, Li G, Moorman JP, Yao ZQ, Ning S. 2017. LMP1 signaling pathway activates IRF4 in latent EBV infection and a positive circuit between PI3K and Src is required. Oncogene 36:2265-2274.

88. Wang L, Ning S. 2013. Interferon regulatory factor 4 is activated through c-Src-mediated tyrosine phosphorylation in virus-transformed cells. J Virol 87:9672-9.

89. Dirmeier U, Hoffmann R, Kilger E, Schultheiss U, Briseño C, Gires O, Kieser A, Eick D, Sugden B, Hammerschmidt W. 2005. Latent membrane protein 1 of Epstein-Barr virus coordinately regulates proliferation with control of apoptosis. Oncogene 24:1711-7.

90. Choi IK, Wang Z, Ke Q, Hong M, Paul DW, Jr., Fernandes SM, Hu Z, Stevens J, Guleria I, Kim HJ, Cantor H, Wucherpfennig KW, Brown JR, Ritz J, Zhang B. 2021. Mechanism of EBV inducing anti-tumour immunity and its therapeutic use. Nature 590:157-162.

91. Mann KP, Staunton D, Thorley-Lawson DA. 1985. Epstein-Barr virus-encoded protein found in plasma membranes of transformed cells. J Virol 55:710-20.

92. Dobin A, Davis CA, Schlesinger F, Drenkow J, Zaleski C, Jha S, Batut P, Chaisson M, Gingeras TR. 2012. STAR: ultrafast universal RNA-seq aligner. Bioinformatics 29:15-21.

93. Liao Y, Smyth GK, Shi W. 2013. featureCounts: an efficient general purpose program for assigning sequence reads to genomic features. Bioinformatics 30:923-930.

94. Love MI, Huber W, Anders S. 2014. Moderated estimation of fold change and dispersion for RNA-seq data with DESeq2. Genome Biol 15:550.

95. Subramanian A, Tamayo P, Mootha VK, Mukherjee S, Ebert BL, Gillette MA, Paulovich A, Pomeroy SL, Golub TR, Lander ES, Mesirov JP. 2005. Gene set enrichment analysis: a knowledge-based approach for interpreting genome-wide expression profiles. Proc Natl Acad Sci U S A 102:15545-50.

96. Reimand J, Isserlin R, Voisin V, Kucera M, Tannus-Lopes C, Rostamianfar A, Wadi L, Meyer M, Wong J, Xu C, Merico D, Bader GD. 2019. Pathway enrichment analysis and visualization of omics data using g:Profiler, GSEA, Cytoscape and EnrichmentMap. Nat Protoc 14:482-517.

Figure 1

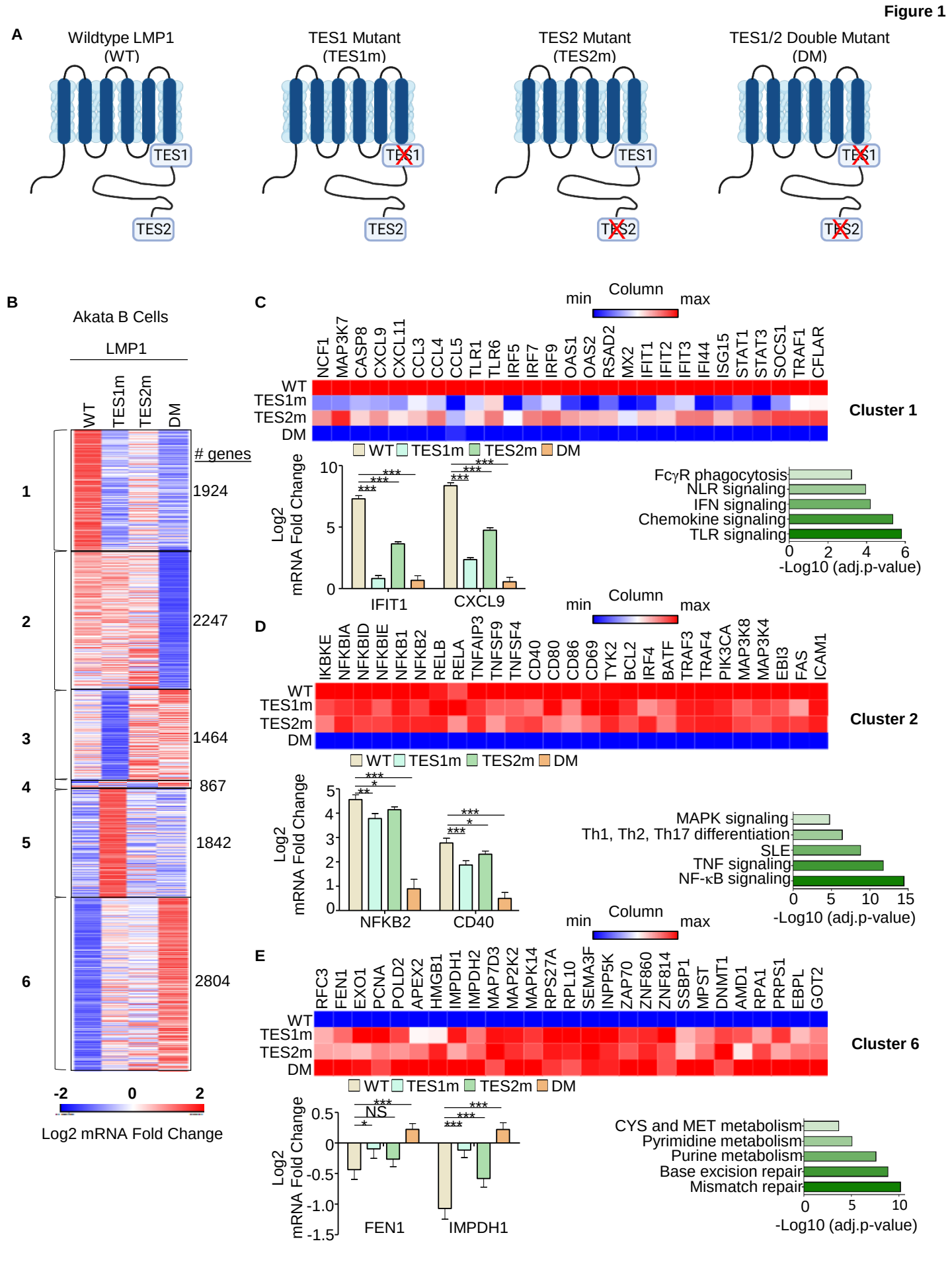
A
Wildtype LMP1 (WT)
TES1 Mutant (TES1m)
TES2 Mutant (TES2m)
TES1/2 Double Mutant (DM)
TES1
TES2
B
Akata B Cells
LMP1
WT
TES1m
TES2m
DM
genes
1
1924
2
2247
3
1464
4
867
5
1842
6
2804
-2
0
2
Log2 mRNA Fold Change
C
Column
min
max
NCF1 MAP3K7 CASP8 CXCL9 CXCL11 CCL3 CCL4 CCL5 TLR1 TLR6 IRF5 IRF7 IRF9 OAS1 OAS2 RSAD2 MX2 IFIT1 IFIT2 IFIT3 IFI44 ISG15 STAT1 STAT3 SOCS1 TRAF1 CFLAR
Cluster 1
Log2 mRNA Fold Change
IFIT1
CXCL9
FcγR phagocytosis
NLR signaling
IFN signaling
Chemokine signaling
TLR signaling
-Log10 (adj.p-value)
D
IKBKE NFKBIA NFKBID NFKBIE NFKB1 NFKB2 RELB RELA TNFAIP3 TNFSF9 TNFSF4 CD40 CD80 CD86 CD69 TYK2 BCL2 IRF4 BATF TRAF3 TRAF4 PIK3CA MAP3K8 MAP3K4 EBI3 FAS ICAM1
Cluster 2
NFKB2
CD40
MAPK signaling
Th1, Th2, Th17 differentiation
SLE
TNF signaling
NF-κB signaling
E
RFC3 FEN1 EXO1 PCNA POLD2 APEX2 HMGB1 IMPDH1 IMPDH2 MAP7D3 MAP2K2 MAPK14 RPS27A RPL10 SEMA3F INPP5K ZAP70 ZNF860 ZNF814 SSBP1 MPST DNMT1 AMD1 RPA1 PRPS1 EBPL GOT2
Cluster 6
FEN1
IMPDH1
NS
CYS and MET metabolism
Pyrimidine metabolism
Purine metabolism
Base excision repair
Mismatch repair

Fig. 1 RNAseq analysis of Akata B-cell responses to WT, TES1, TES2 or DM LMP1.

(A) Schematic diagram of LMP1 WT, TES1m, TES2m and DM.

(B) K-means heatmap of transcriptome responses in EBV- Akata cells to LMP1 WT, TES1m, TES2m or DM expression induced by 250 ng/ml doxycycline for 24 hours. Heatmap depicts RNAseq of host gene Log2 Fold change across n=3 independent replicates, divided into six clusters. A two-way ANOVA P value cutoff of <0.01 and >2-fold gene expression were used.

(C) Heatmaps of representative Cluster 1 differentially regulated genes (top). Also shown are expression values of two representative Clusters 1 genes (lower left) and Enrichr KEGG pathway –Log 10 (adjusted p values) of significantly enriched Cluster 1 gene sets (lower right). p-values were determined by one-sided Fisher's exact test. ***p<0.001.

(D) Heatmaps of representative Cluster 2 differentially regulated genes (top). Also shown are expression values of two representative Clusters 2 genes (lower left) and Enrichr KEGG pathway –Log 10 (adjusted p values) of significantly enriched Cluster 2 gene sets (lower right). p-values were determined by one-sided Fisher's exact test. *p<0.05, **p<0.01, ***p<0.001.

(E) Heatmaps of representative Cluster 6 differentially regulated genes (top). Also shown are expression values of two representative Clusters 6 genes (lower left) and Enrichr KEGG pathway –Log 10 (adjusted p values) of significantly enriched Cluster 6 gene sets (lower right). p-values were determined by one-sided Fisher's exact test. *p<0.05, ***p<0.001.

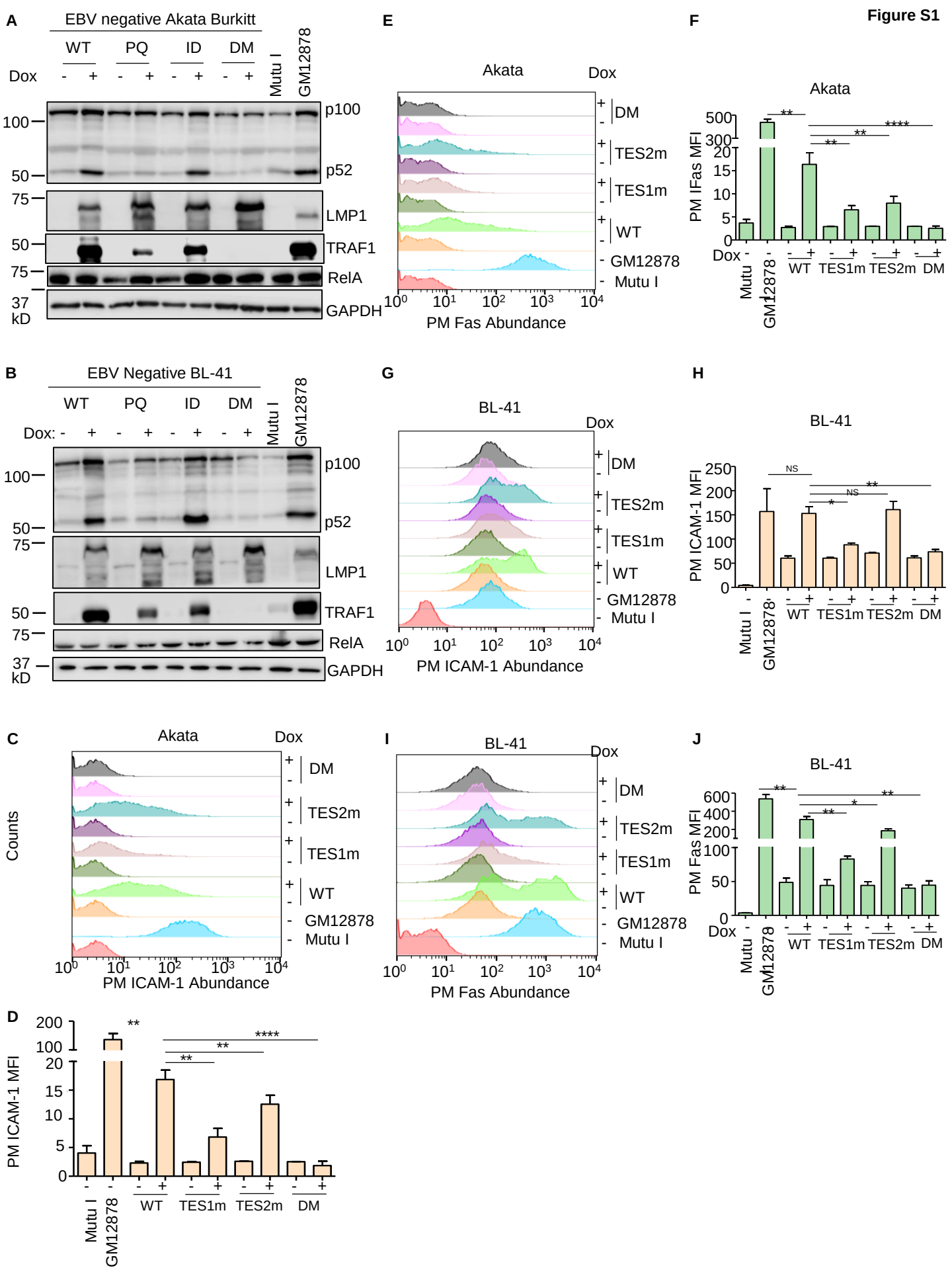
Figure S1
A
EBV negative Akata Burkitt
WT
PQ
ID
DM
Dox
Mutu I
GM12878
p100
p52
LMP1
TRAF1
RelA
GAPDH
37 kD
B
EBV Negative BL-41
Dox:
C
Akata
Counts
PM ICAM-1 Abundance
D
PM ICAM-1 MFI
E
Akata
PM Fas Abundance
F
PM IFas MFI
G
BL-41
PM ICAM-1 Abundance
H
PM ICAM-1 MFI
I
BL-41
PM Fas Abundance
J
PM Fas MFI
TES2m
TES1m
NS

Fig. S1 Analysis of LMP1 WT, TES1m, TES2m and DM effects in EBV-negative Akata B-cells.

(A) Immunoblot analysis of whole cell lysates (WCL) in Akata cells induced for LMP1 as indicated by 250 ng/ml doxycycline (Dox) for 24 hours. Blots are representative of n = 3 experiments.

(B) Immunoblot analysis of whole cell lysates (WCL) in BL-41 cells induced for LMP1 as indicated. Blots are representative of n = 3 experiments.

(C) FACS analysis of plasma membrane (PM) ICAM-1 in Akata cells induced for LMP1 by 250 ng/ml dox for 24 hours, as indicated. For comparison, levels in GM12878 LCLs or latency I Mutu I Burkitt cells are shown.

(D) PM ICAM-1 Mean Fluorescence Intensity (MFI) + SD in Akata cells with the indicated LMP1 expression, as in (C). p-values were determined by one-sided Fisher's exact test. **$p<0.001$, ***$p<0.0001$.

(E) PM Fas MFI in Akata cells induced for LMP1 by 250ng/ml of dox for 24 hours as indicated. For comparison, levels in GM12878 LCLs or latency I Mutu I Burkitt cells are shown.

(F) PM Fas MFI + SD in Akata cells with the indicated LMP1 expression, as in (E). P-values were determined by one-sided Fisher's exact test. **$p<0.001$, ***$p<0.0001$.

(G) PM ICAM-1 MFI + SD in BL-41 cells induced for LMP1 expression by 250ng/ml dox for 24 hours, as indicated. p-values were determined by one-sided Fisher's exact test. **$p<0.001$, ***$p<0.0001$.

(H) PM ICAM-1 MFI + SD in Akata cells with the indicated LMP1 expression, as in (G). P-values were determined by one-sided Fisher's exact test. **$p<0.001$, ***$p<0.0001$.

(I)PM Fas MFI + SD in BL-41 cells induced for LMP1 expression by 250 ng/ml dox for 24 hours, as indicated. p-values were determined by one-sided Fisher's exact test. **$p<0.001$, ***$p<0.0001$.

(J) Mean Fluorescence Intensity (MFI) presented for Fas+ population in BL-41-LMP1 cells, , as in (I). p-values were determined by one-sided Fisher's exact test. **$p<0.001$, ***$p<0.0001$.

Figure S2

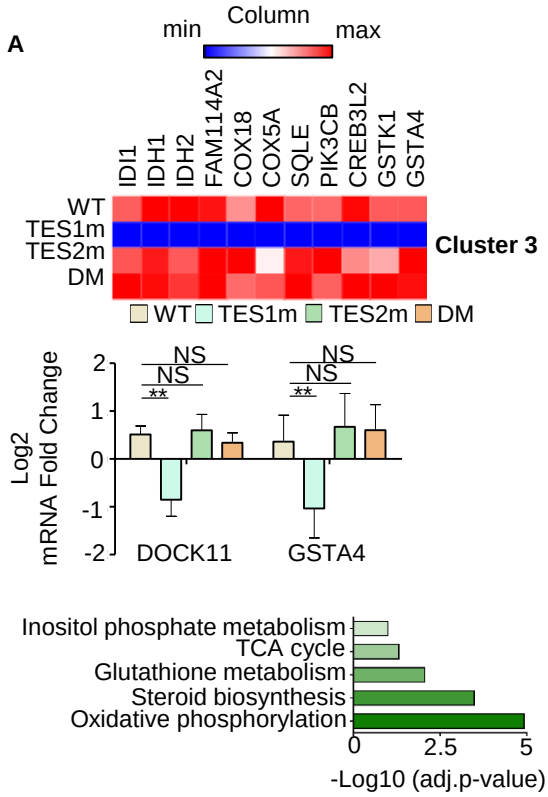
A
Column
min
max
IDI1
IDH1
IDH2
FAM114A2
COX18
COX5A
SQLE
PIK3CB
CREB3L2
GSTK1
GSTA4
WT
TES1m
TES2m
DM
Cluster 3
WT TES1m TES2m DM
Log2 mRNA Fold Change
NS
NS
**
NS
NS
**
DOCK11
GSTA4
Inositol phosphate metabolism
TCA cycle
Glutathione metabolism
Steroid biosynthesis
Oxidative phosphorylation
-Log10 (adj.p-value)

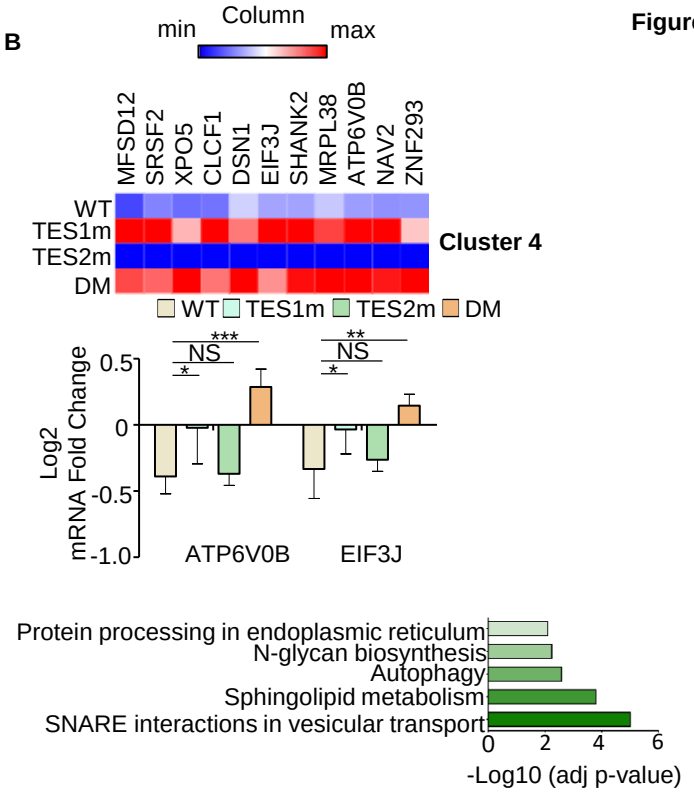
B
Column
min
max
MFSD12
SRSF2
XPO5
CLCF1
DSN1
EIF3J
SHANK2
MRPL38
ATP6V0B
NAV2
ZNF293
WT
TES1m
TES2m
DM
Cluster 4
WT TES1m TES2m DM
Log2 mRNA Fold Change
***
NS
*
**
NS
*
ATP6V0B
EIF3J
Protein processing in endoplasmic reticulum
N-glycan biosynthesis
Autophagy
Sphingolipid metabolism
SNARE interactions in vesicular transport
-Log10 (adj p-value)

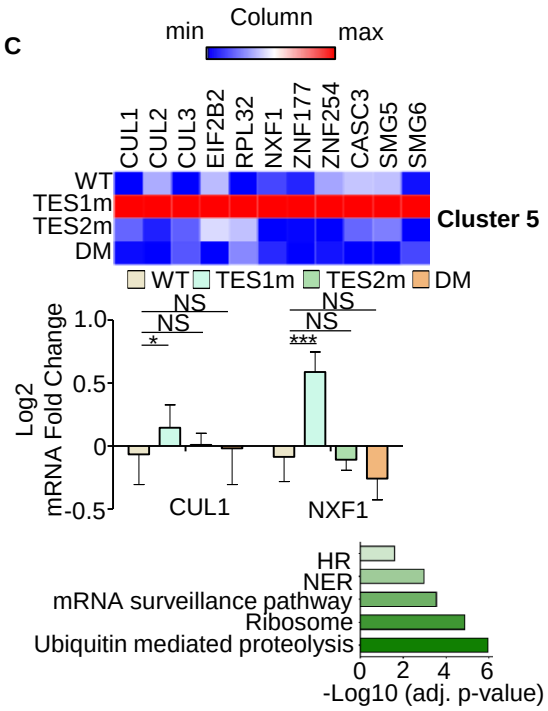
C
Column
min
max
CUL1
CUL2
CUL3
EIF2B2
RPL32
NXF1
ZNF177
ZNF254
CASC3
SMG5
SMG6
WT
TES1m
TES2m
DM
Cluster 5
WT TES1m TES2m DM
Log2 mRNA Fold Change
NS
NS
*
NS
NS
***
CUL1
NXF1
HR
NER
mRNA surveillance pathway
Ribosome
Ubiquitin mediated proteolysis
-Log10 (adj. p-value)

Fig. S2. RNAseq analysis of Akata B-cell responses to WT, TES1, TES2 or DM LMP1.

(A) Heatmaps of representative Cluster 3 differentially regulated genes (top). Also shown are expression values of two representative Clusters 3 genes (lower left) and Enrichr KEGG pathway –Log 10 (adjusted p values) of significantly enriched Cluster 3 gene sets (lower right). p-values were determined by one-sided Fisher's exact test. **p<0.01.

(B) Heatmaps of representative Cluster 4 differentially regulated genes (top). Also shown are expression values of two representative Clusters 4 genes (lower left) and Enrichr KEGG pathway –Log 10 (adjusted p values) of significantly enriched Cluster 4 gene sets (lower right). p-values were determined by one-sided Fisher's exact test. *p<0.05, **p<0.01, ***p<0.001.

(C) Heatmaps of representative Cluster 5 differentially regulated genes (top). Also shown are expression values of two representative Clusters 5 genes (lower left) and Enrichr KEGG pathway –Log 10 (adjusted p values) of significantly enriched Cluster 5 gene sets (lower right). p-values were determined by one-sided Fisher's exact test. *p<0.05, ***p<0.001.

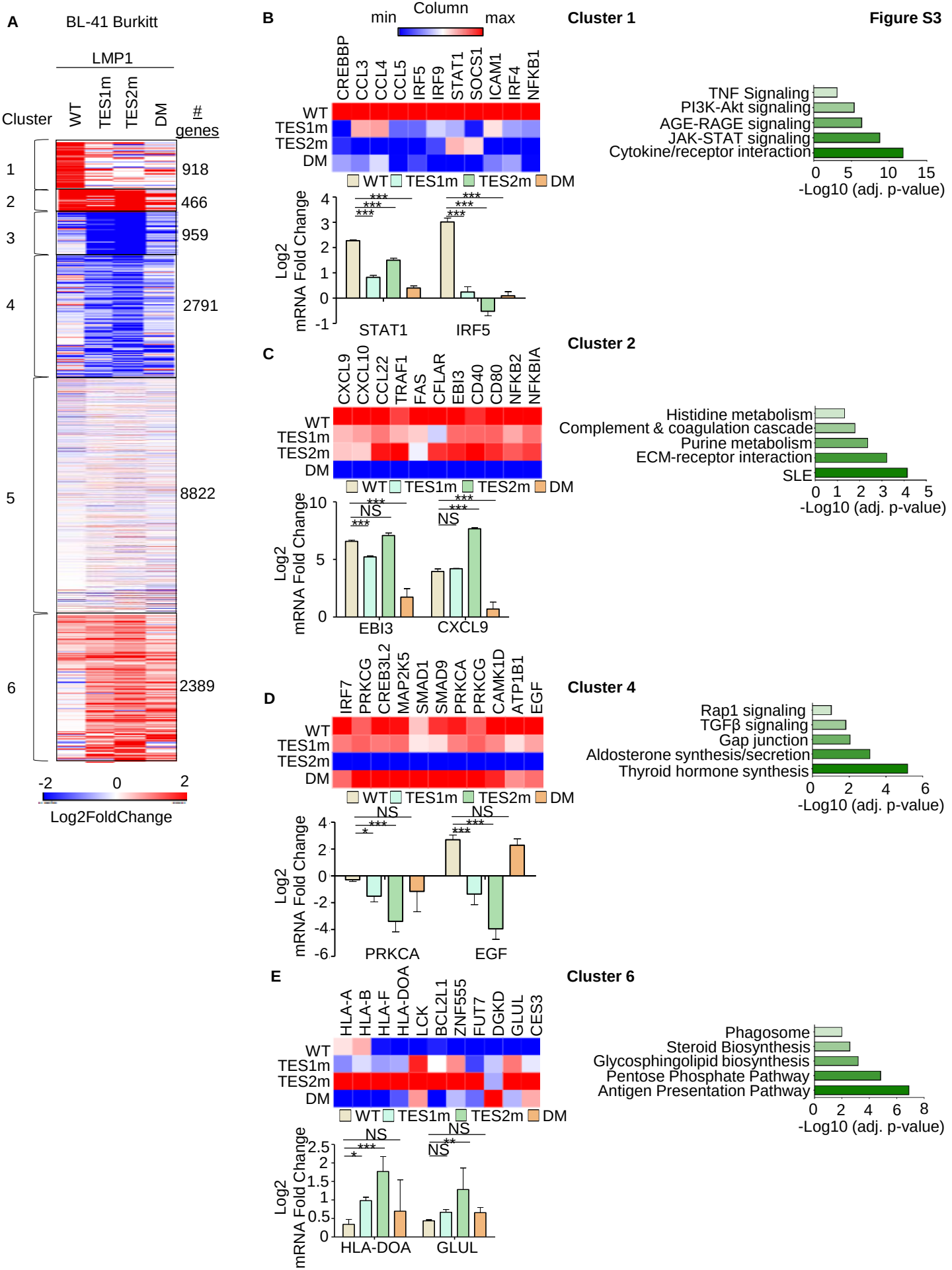
Figure S3
A
BL-41 Burkitt
LMP1
Cluster
WT
TES1m
TES2m
DM
genes
1
2
3
4
5
6
918
466
959
2791
8822
2389
-2
0
2
Log2FoldChange
B
Column
min
max
Cluster 1
CREBBP
CCL3
CCL4
CCL5
IRF5
IRF9
STAT1
SOCS1
ICAM1
IRF4
NFKB1
WT
TES1m
TES2m
DM
Log2 mRNA Fold Change
STAT1
IRF5
TNF Signaling
PI3K-Akt signaling
AGE-RAGE signaling
JAK-STAT signaling
Cytokine/receptor interaction
-Log10 (adj. p-value)
C
Cluster 2
CXCL9
CXCL10
CCL22
TRAF1
FAS
CFLAR
EBI3
CD40
CD80
NFKB2
NFKBIA
EBI3
CXCL9
Histidine metabolism
Complement & coagulation cascade
Purine metabolism
ECM-receptor interaction
SLE
-Log10 (adj. p-value)
D
Cluster 4
IRF7
PRKCG
CREB3L2
MAP2K5
SMAD1
SMAD9
PRKCA
PRKCG
CAMK1D
ATP1B1
EGF
PRKCA
EGF
Rap1 signaling
TGFβ signaling
Gap junction
Aldosterone synthesis/secretion
Thyroid hormone synthesis
-Log10 (adj. p-value)
E
Cluster 6
HLA-A
HLA-B
HLA-F
HLA-DOA
LCK
BCL2L1
ZNF555
FUT7
DGKD
GLUL
CES3
HLA-DOA
GLUL
Phagosome
Steroid Biosynthesis
Glycosphingolipid biosynthesis
Pentose Phosphate Pathway
Antigen Presentation Pathway
-Log10 (adj. p-value)

Fig. S3 RNAseq analysis of BL-41 B-cell responses to WT, TES1, TES2 or DM LMP1.

(A) K-means heatmap of transcriptome responses in EBV- BL-41 cells to LMP1 WT, TES1m, TES2m or DM expression induced by 250 ng/ml doxycycline for 24 hours. Heatmap depicts RNAseq of host gene Log2 Fold change across n=3 independent replicates, divided into six clusters. A two-way ANOVA P value cutoff of <0.01 and >2-fold gene expression were used.

(B) Heatmaps of representative Cluster 1 differentially regulated genes (top). Also shown are expression values of two representative Clusters 1 genes (lower left) and Enrichr KEGG pathway –Log 10 (adjusted p values) of significantly enriched Cluster 1 gene sets (lower right). p-values were determined by one-sided Fisher's exact test. ***p<0.001.

(C) Heatmaps of representative Cluster 2 differentially regulated genes (top). Also shown are expression values of two representative Clusters 2 genes (lower left) and Enrichr KEGG pathway –Log 10 (adjusted p values) of significantly enriched Cluster 2 gene sets (lower right). p-values were determined by one-sided Fisher's exact test. ***p<0.001.

(D) Heatmaps of representative Cluster 4 differentially regulated genes (top). Also shown are expression values of two representative Clusters 4 genes (lower left) and Enrichr KEGG pathway –Log 10 (adjusted p values) of significantly enriched Cluster 4 gene sets (lower right). p-values were determined by one-sided Fisher's exact test. *p<0.05, ***p<0.001.

(E) Heatmaps of representative Cluster 6 differentially regulated genes (top). Also shown are expression values of two representative Clusters 6 genes (lower left) and Enrichr KEGG pathway –Log 10 (adjusted p values) of significantly enriched Cluster 6 gene sets (lower right). p-values were determined by one-sided Fisher's exact test. *p<0.05, **p<0.01, ***p<0.001.

Figure 2

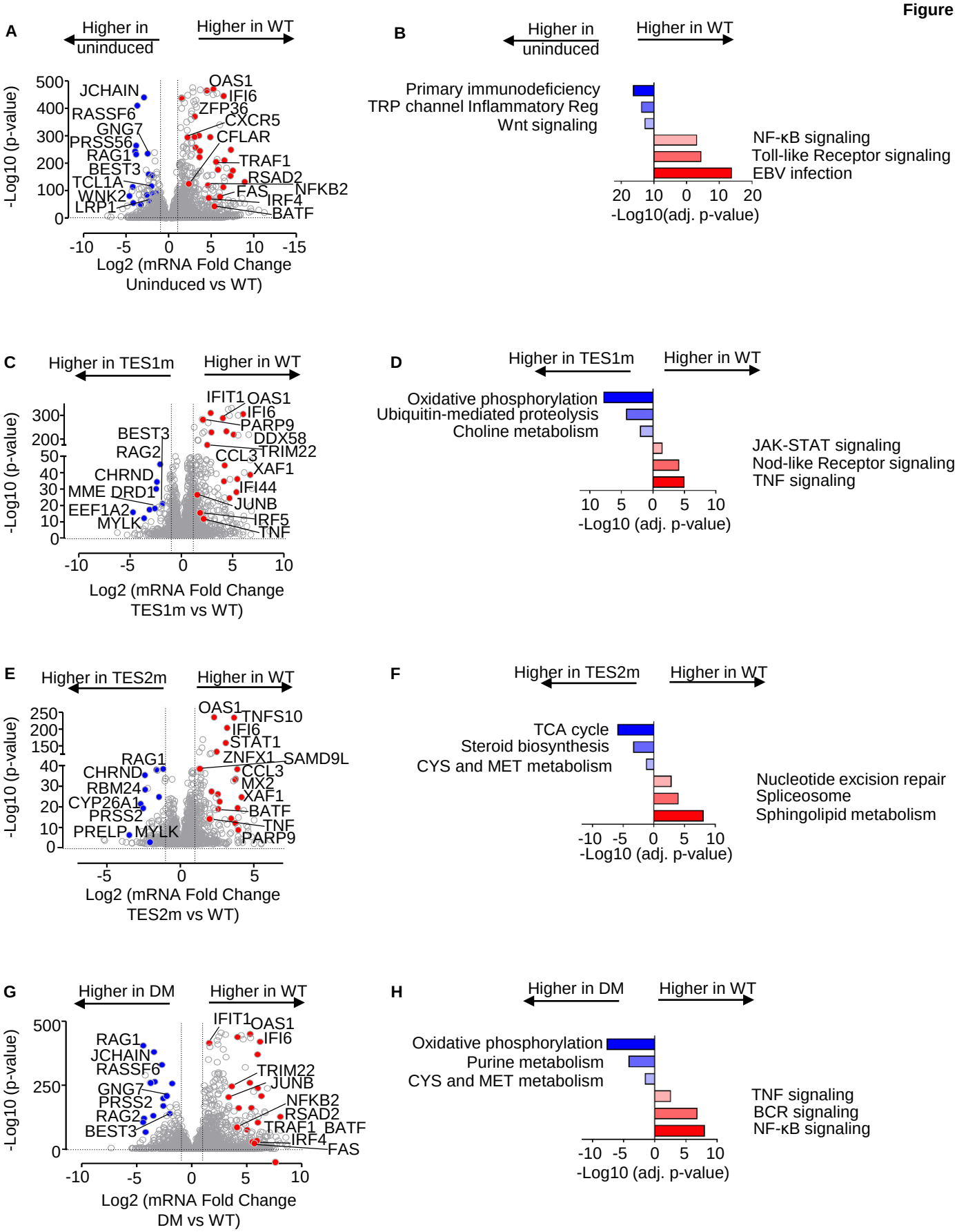
A
Higher in uninduced
Higher in WT
-Log10 (p-value)
JCHAIN
RASSF6
GNG7
PRSS56
RAG1
BEST3
TCL1A
WNK2
LRP1
OAS1
IFI6
ZFP36
CXCR5
CFLAR
TRAF1
RSAD2
FAS
NFKB2
IRF4
BATF
Log2 (mRNA Fold Change Uninduced vs WT)
B
Higher in uninduced
Higher in WT
Primary immunodeficiency
TRP channel Inflammatory Reg
Wnt signaling
NF-κB signaling
Toll-like Receptor signaling
EBV infection
-Log10(adj. p-value)
C
Higher in TES1m
Higher in WT
-Log10 (p-value)
BEST3
RAG2
CHRND
MME
DRD1
EEF1A2
MYLK
IFIT1
OAS1
IFI6
PARP9
DDX58
TRIM22
CCL3
XAF1
IFI44
JUNB
IRF5
TNF
Log2 (mRNA Fold Change TES1m vs WT)
D
Higher in TES1m
Higher in WT
Oxidative phosphorylation
Ubiquitin-mediated proteolysis
Choline metabolism
JAK-STAT signaling
Nod-like Receptor signaling
TNF signaling
-Log10 (adj. p-value)
E
Higher in TES2m
Higher in WT
-Log10 (p-value)
RAG1
CHRND
RBM24
CYP26A1
PRSS2
PRELP
MYLK
OAS1
TNFS10
IFI6
STAT1
ZNFX1
SAMD9L
CCL3
MX2
XAF1
BATF
TNF
PARP9
Log2 (mRNA Fold Change TES2m vs WT)
F
Higher in TES2m
Higher in WT
TCA cycle
Steroid biosynthesis
CYS and MET metabolism
Nucleotide excision repair
Spliceosome
Sphingolipid metabolism
-Log10 (adj. p-value)
G
Higher in DM
Higher in WT
-Log10 (p-value)
RAG1
JCHAIN
RASSF6
GNG7
PRSS2
RAG2
BEST3
IFIT1
OAS1
IFI6
TRIM22
JUNB
NFKB2
RSAD2
TRAF1
BATF
IRF4
FAS
Log2 (mRNA Fold Change DM vs WT)
H
Higher in DM
Higher in WT
Oxidative phosphorylation
Purine metabolism
CYS and MET metabolism
TNF signaling
BCR signaling
NF-κB signaling
-Log10 (adj. p-value)

Fig. 2. Effects of LMP1 signaling on the Akata transcriptome.

(A) Volcano plot analysis of Akata RNA-seq, comparing mRNA values in cells induced for LMP1 WT for 24 hours vs. mock-induced.

(B) Enrichr KEGG pathways most highly changed in WT versus uninduced Akata, as in (A).

(C) Volcano plot analysis of Akata RNA-seq, comparing mRNA values in cells induced for LMP1 WT vs LMP1 TES1m for 24 hours.

(D) Enrichr KEGG pathways most highly changed with WT versus LMP1 TES1m expression, as in (C).

(E) Volcano plot analysis of Akata RNA-seq, comparing mRNA values in cells induced for LMP1 WT vs LMP1 TES2m for 24 hours.

(F) Enrichr KEGG pathways most highly changed with WT versus LMP1 TES2m expression, as in (E).

(G) Volcano plot analysis of Akata RNA-seq, comparing mRNA values in cells induced for LMP1 WT vs LMP1 DM for 24 hours.

(H) Enrichr KEGG pathways most highly changed with WT versus LMP1 DM expression, as in (G).

Figure S4

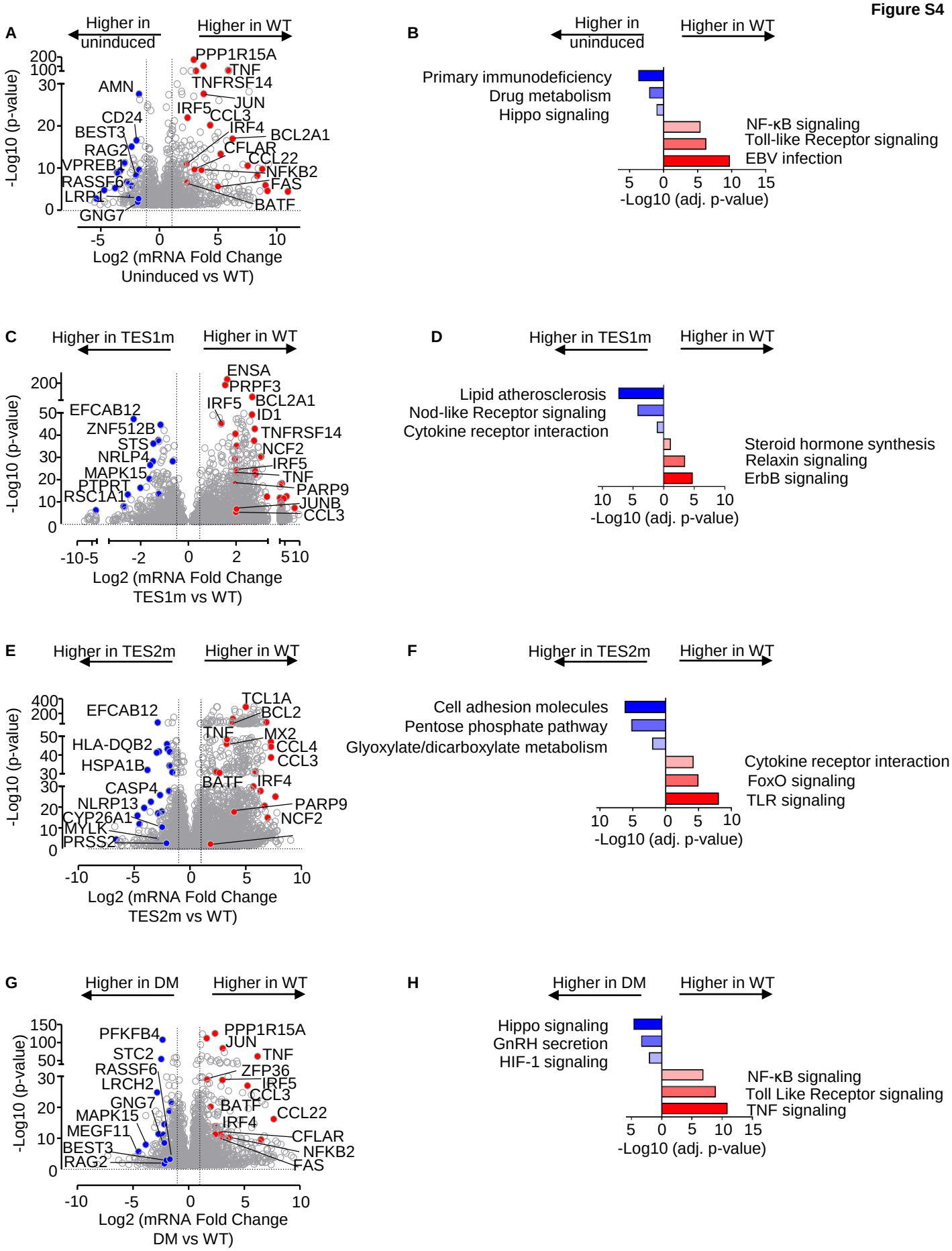
A
Higher in uninduced
Higher in WT
-Log10 (p-value)
Log2 (mRNA Fold Change Uninduced vs WT)
PPP1R15A
TNF
TNFRSF14
JUN
IRF5
CCL3
IRF4
BCL2A1
CFLAR
CCL22
NFKB2
FAS
BATF
AMN
CD24
BEST3
RAG2
VPREB1
RASSF6
LRP1
GNG7
B
Higher in uninduced
Higher in WT
Primary immunodeficiency
Drug metabolism
Hippo signaling
NF-κB signaling
Toll-like Receptor signaling
EBV infection
-Log10 (adj. p-value)
C
Higher in TES1m
Higher in WT
-Log10 (p-value)
Log2 (mRNA Fold Change TES1m vs WT)
ENSA
PRPF3
BCL2A1
IRF5
ID1
TNFRSF14
NCF2
IRF5
TNF
PARP9
JUNB
CCL3
EFCAB12
ZNF512B
STS
NRLP4
MAPK15
PTPRT
RSC1A1
D
Higher in TES1m
Higher in WT
Lipid atherosclerosis
Nod-like Receptor signaling
Cytokine receptor interaction
Steroid hormone synthesis
Relaxin signaling
ErbB signaling
-Log10 (adj. p-value)
E
Higher in TES2m
Higher in WT
-Log10 (p-value)
Log2 (mRNA Fold Change TES2m vs WT)
TCL1A
BCL2
TNF
MX2
CCL4
CCL3
BATF
IRF4
PARP9
NCF2
EFCAB12
HLA-DQB2
HSPA1B
CASP4
NLRP13
CYP26A1
MYLK
PRSS2
F
Higher in TES2m
Higher in WT
Cell adhesion molecules
Pentose phosphate pathway
Glyoxylate/dicarboxylate metabolism
Cytokine receptor interaction
FoxO signaling
TLR signaling
-Log10 (adj. p-value)
G
Higher in DM
Higher in WT
-Log10 (p-value)
Log2 (mRNA Fold Change DM vs WT)
PPP1R15A
JUN
TNF
ZFP36
IRF5
CCL3
BATF
IRF4
CCL22
CFLAR
NFKB2
FAS
PFKFB4
STC2
RASSF6
LRCH2
GNG7
MAPK15
MEGF11
BEST3
RAG2
H
Higher in DM
Higher in WT
Hippo signaling
GnRH secretion
HIF-1 signaling
NF-κB signaling
Toll Like Receptor signaling
TNF signaling
-Log10 (adj. p-value)

Fig. S4. Effects of LMP1 signaling on the BL-41 transcriptome.

(A) Volcano plot analysis of BL-41 RNA-seq, comparing mRNA values in cells induced for LMP1 WT for 24 hours vs. mock-induced.

(B) Enrichr KEGG pathways most highly changed in WT versus uninduced BL-41, as in (A).

(C) Volcano plot analysis of BL-41 RNA-seq, comparing mRNA values in cells induced for LMP1 WT vs LMP1 TES1m for 24 hours.

(D) Enrichr KEGG pathways most highly changed with WT versus LMP1 TES1m expression, as in (C).

(E) Volcano plot analysis of BL-41 RNA-seq, comparing mRNA values in cells induced for LMP1 WT vs LMP1 TES2m for 24 hours.

(F) Enrichr KEGG pathways most highly changed with WT versus LMP1 TES2m expression, as in (E).

(G) Volcano plot analysis of BL-41 RNA-seq, comparing mRNA values in cells induced for LMP1 WT vs LMP1 DM for 24 hours.

(H) Enrichr KEGG pathways most highly changed with WT versus LMP1 DM expression, as in (G).

Figure 3

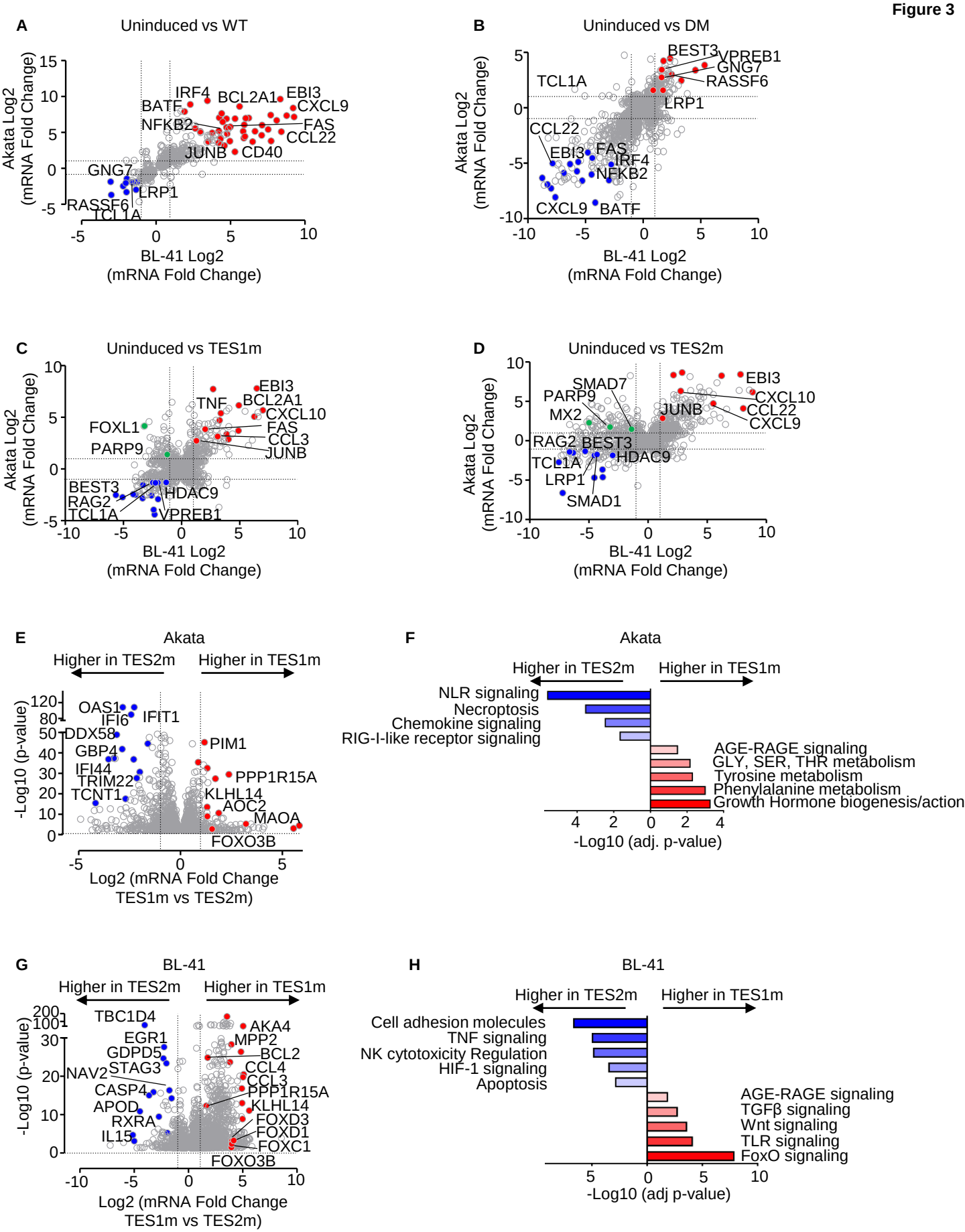
A
Uninduced vs WT
Akata Log2 (mRNA Fold Change)
BL-41 Log2 (mRNA Fold Change)
IRF4
BCL2A1
EBI3
CXCL9
BATF
NFKB2
FAS
CCL22
JUNB
CD40
GNG7
LRP1
RASSF6
TCL1A
B
Uninduced vs DM
BEST3
VPREB1
GNG7
RASSF6
TCL1A
LRP1
CCL22
EBI3
FAS
IRF4
NFKB2
CXCL9
BATF
C
Uninduced vs TES1m
EBI3
TNF
BCL2A1
CXCL10
FOXL1
FAS
CCL3
PARP9
JUNB
BEST3
HDAC9
RAG2
TCL1A
VPREB1
D
Uninduced vs TES2m
SMAD7
EBI3
PARP9
CXCL10
MX2
JUNB
CCL22
CXCL9
RAG2
BEST3
HDAC9
TCL1A
LRP1
SMAD1
E
Akata
Higher in TES2m
Higher in TES1m
-Log10 (p-value)
OAS1
IFI6
IFIT1
DDX58
PIM1
GBP4
IFI44
PPP1R15A
TRIM22
TCNT1
KLHL14
AOC2
MAOA
FOXO3B
Log2 (mRNA Fold Change TES1m vs TES2m)
F
Akata
Higher in TES2m
Higher in TES1m
NLR signaling
Necroptosis
Chemokine signaling
RIG-I-like receptor signaling
AGE-RAGE signaling
GLY, SER, THR metabolism
Tyrosine metabolism
Phenylalanine metabolism
Growth Hormone biogenesis/action
-Log10 (adj. p-value)
G
BL-41
Higher in TES2m
Higher in TES1m
-Log10 (p-value)
TBC1D4
AKA4
EGR1
MPP2
GDPD5
BCL2
NAV2
STAG3
CCL4
CCL3
CASP4
PPP1R15A
APOD
KLHL14
RXRA
FOXD3
IL15
FOXD1
FOXC1
FOXO3B
Log2 (mRNA Fold Change TES1m vs TES2m)
H
BL-41
Higher in TES2m
Higher in TES1m
Cell adhesion molecules
TNF signaling
NK cytotoxicity Regulation
HIF-1 signaling
Apoptosis
AGE-RAGE signaling
TGFβ signaling
Wnt signaling
TLR signaling
FoxO signaling
-Log10 (adj p-value)

Fig. 3. Cross-comparison of target gene induction by LMP signaling in Akata vs BL-41.

(A) Scatter plot analysis of fold changes in mRNA abundances in cells induced for LMP1 WT for 24 hours versus uninduced. Shown are genes differentially regulated by >1 fold.

(B) Scatter plot analysis of fold changes in mRNA abundances in cells induced for LMP1 DM for 24 hours versus uninduced. Shown are genes differentially regulated by >1 fold.

(C) Scatter plot analysis of fold changes in mRNA abundances in cells induced for LMP1 TES1m for 24 hours versus uninduced. Shown are genes differentially regulated by >1 fold.

(D) Scatter plot analysis of fold changes in mRNA abundances in cells induced for LMP1 TES2m for 24 hours versus uninduced. Shown are genes differentially regulated by >1 fold.

(E) Volcano plot analysis of Akata genes differentially regulated by LMP1 TES1m vs TES2m expression for 24 hours.

(F) Enrichr KEGG pathways most highly changed with LMP1 TES1m vs TES2m expression in Akata, as in (E).

(G) Volcano plot analysis of BL-41 genes differentially regulated by LMP1 TES1m vs TES2m expression for 24 hours.

(H) Enrichr KEGG pathways most highly changed with LMP1 TES1m vs TES2m expression in BL-41, as in (G).

Figure S5

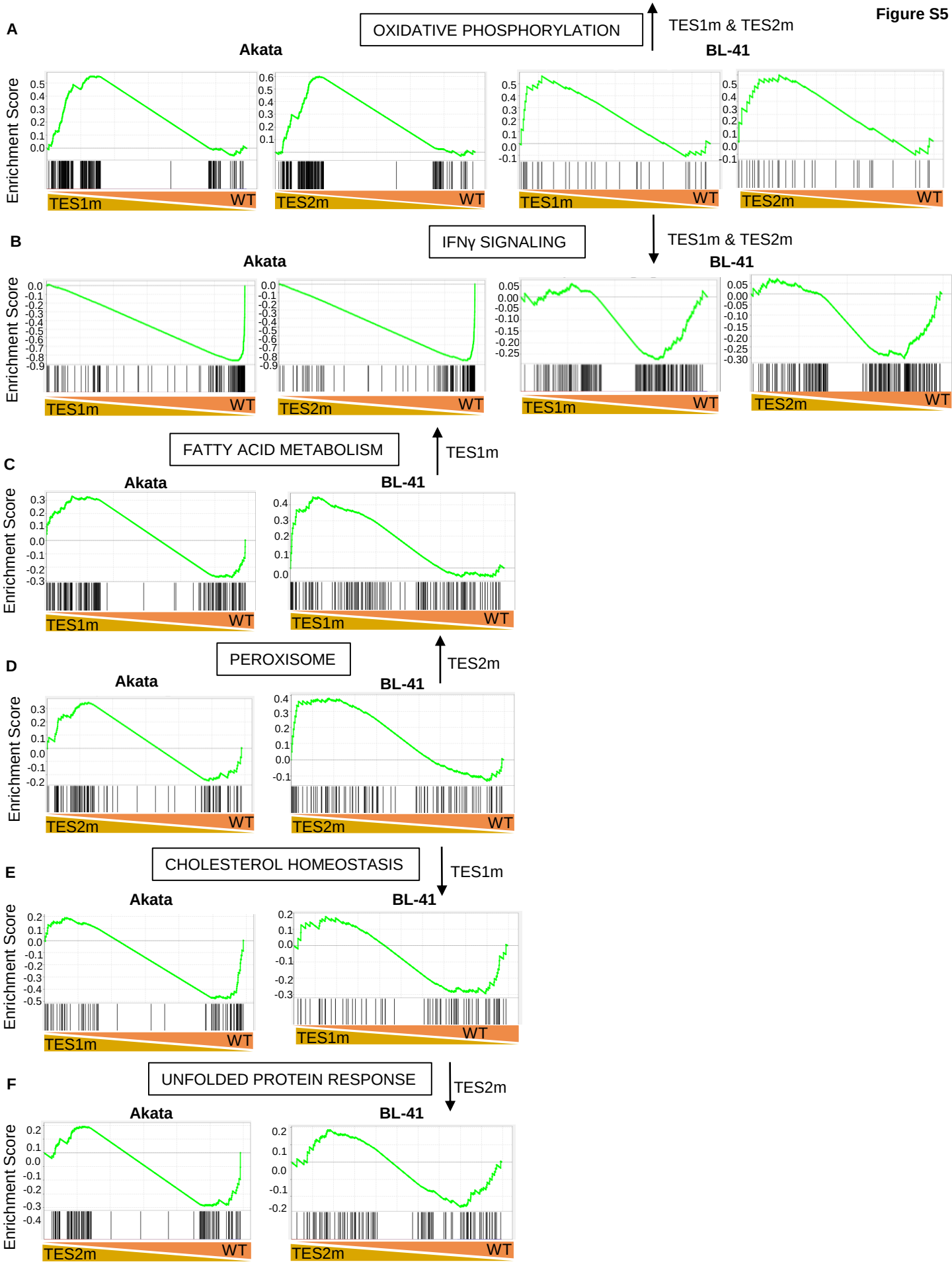
A
OXIDATIVE PHOSPHORYLATION
TES1m & TES2m
Akata
BL-41
Enrichment Score
TES1m
WT
TES2m
WT
TES1m
WT
TES2m
WT
B
IFNγ SIGNALING
TES1m & TES2m
Akata
BL-41
Enrichment Score
TES1m
WT
TES2m
WT
TES1m
WT
TES2m
WT
C
FATTY ACID METABOLISM
TES1m
Akata
BL-41
Enrichment Score
TES1m
WT
TES1m
WT
D
PEROXISOME
TES2m
Akata
BL-41
Enrichment Score
TES2m
WT
TES2m
WT
E
CHOLESTEROL HOMEOSTASIS
TES1m
Akata
BL-41
Enrichment Score
TES1m
WT
TES1m
WT
F
UNFOLDED PROTEIN RESPONSE
TES2m
Akata
BL-41
Enrichment Score
TES2m
WT
TES2m
WT

Fig. S5. GSEA of a subset of pathways differentially regulated by WT vs TES mutant LMP1.

(A) GSEA analysis of oxidative phosphorylation genes in Akata (left) and BL-41 (right) expressing LMP1 as indicated for 24 hours.

(B) GSEA analysis of IFNγ signaling genes in Akata (left) and BL-41 (right) expressing LMP1 as indicated for 24 hours.

(C) GSEA analysis of fatty acid metabolism genes in Akata (left) and BL-41 (right) expressing LMP1 as indicated for 24 hours.

(D) GSEA analysis of peroxisome genes in Akata (left) and BL-41 (right) expressing LMP1 as indicated for 24 hours.

(E) GSEA analysis of cholesterol homeostasis genes in Akata (left) and BL-41 (right) expressing LMP1 as indicated for 24 hours.

(F) GSEA analysis of unfolded protein response genes in Akata (left) and BL-41 (right) expressing LMP1 as indicated for 24 hours.

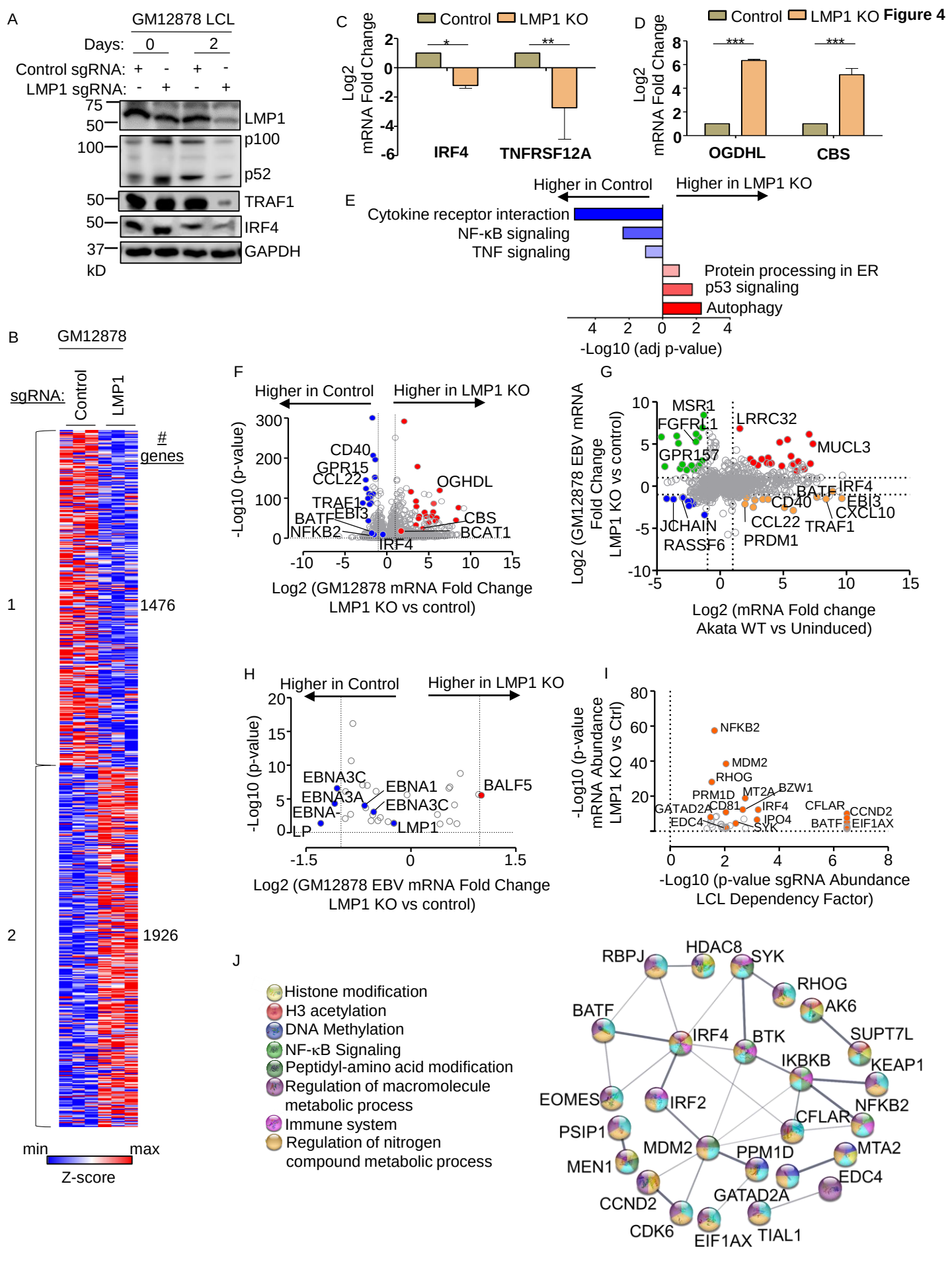
Figure 4
A
GM12878 LCL
Days: 0 2
Control sgRNA: + - + -
LMP1 sgRNA: - + - +
75
50
100
50
50
37
kD
LMP1
p100
p52
TRAF1
IRF4
GAPDH
B
GM12878
sgRNA:
Control
LMP1
genes
1
1476
2
1926
min
max
Z-score
C
Control
LMP1 KO
Log2 mRNA Fold Change
IRF4
TNFRSF12A
D
Control
LMP1 KO
Log2 mRNA Fold Change
OGDHL
CBS
E
Higher in Control
Higher in LMP1 KO
Cytokine receptor interaction
NF-κB signaling
TNF signaling
Protein processing in ER
p53 signaling
Autophagy
-Log10 (adj p-value)
F
Higher in Control
Higher in LMP1 KO
-Log10 (p-value)
CD40
GPR15
CCL22
TRAF1
EBI3
BATF
NFKB2
IRF4
OGHDL
CBS
BCAT1
Log2 (GM12878 mRNA Fold Change LMP1 KO vs control)
G
Log2 (GM12878 EBV mRNA Fold Change LMP1 KO vs control)
MSR1
FGFRL1
GPR157
LRRC32
MUCL3
BATF
IRF4
CD40
EBI3
CXCL10
JCHAIN
CCL22
TRAF1
RASSF6
PRDM1
Log2 (mRNA Fold change Akata WT vs Uninduced)
H
Higher in Control
Higher in LMP1 KO
-Log10 (p-value)
EBNA3C
EBNA3A
EBNA-LP
EBNA1
EBNA3C
LMP1
BALF5
Log2 (GM12878 EBV mRNA Fold Change LMP1 KO vs control)
I
-Log10 (p-value mRNA Abundance LMP1 KO vs Ctrl)
NFKB2
MDM2
RHOG
PRM1D
MT2A
BZW1
GATAD2A
CD81
IRF4
CFLAR
CCND2
EDC4
IPO4
BATF
EIF1AX
SYK
-Log10 (p-value sgRNA Abundance LCL Dependency Factor)
J
Histone modification
H3 acetylation
DNA Methylation
NF-κB Signaling
Peptidyl-amino acid modification
Regulation of macromolecule metabolic process
Immune system
Regulation of nitrogen compound metabolic process
RBPJ
HDAC8
SYK
RHOG
AK6
BATF
IRF4
BTK
SUPT7L
IKBKB
KEAP1
EOMES
IRF2
NFKB2
CFLAR
PSIP1
MDM2
PPM1D
MTA2
MEN1
EDC4
GATAD2A
CCND2
CDK6
EIF1AX
TIAL1

Fig. 4 CRISPR LMP1 KO effects on GM12878 LCL target gene regulation.

(A) Immunoblot analysis of WCL from GM12878 LCLs expressing control or LMP1 targeting sgRNAs and puromycin selected for 0 vs 2 days, as indicated. Blots are representative of n = 3 experiments.

(B) K-means heatmap of transcriptome responses in Latency III GM12878 LCL expressing control or LMP1 sgRNA and puromycin selected for 48 hours, as indicated. Heatmap depicts relative row Z-scores from n=3 independent RNAseq replicates, divided into two clusters. Two-way ANOVA P value cutoff of <0.01 and >2-fold gene expression cutoffs were used.

(C) Values of two representative Clusters 1 genes. p-values were determined by one-sided Fisher's exact test. *p<0.05, **p<0.01.

(D) Values of two representative Clusters 2 genes. p-values were determined by one-sided Fisher's exact test. ***p<0.001.

(E) Enrichr KEGG pathways most highly changed with LMP1 KO.

(F) Volcano plot analysis of GM12878 genes differentially regulated by LMP1 KO, as in (B).

(G) Scatter plot analysis cross comparing mRNA abundance fold changes in LMP1 sgRNA vs control (Y-axis) versus Akata expressing LMP1 WT for 24 hours vs uninduced (x-axis). Shown are genes differentially regulated by >1 fold.

(H) Volcano plot analysis of EBV mRNA values in GM12878 expressing LMP1 vs control sgRNAs, as in (B). P-value cutoff of <0.05 and >1-fold gene expression were used.

(I) Scatter plot analysis cross comparing -Log10 p-values of GM12878 with LMP1 vs control sgRNA (Y-axis) versus CRISPR LCL vs Burkitt cell dependency factor analysis from (25) (X-axis). Shown are genes with p<0.05 in both analyses.

(J) String analysis of genes shown in (I). Respective pathways for each gene and interaction are colored coded.

Figure S6

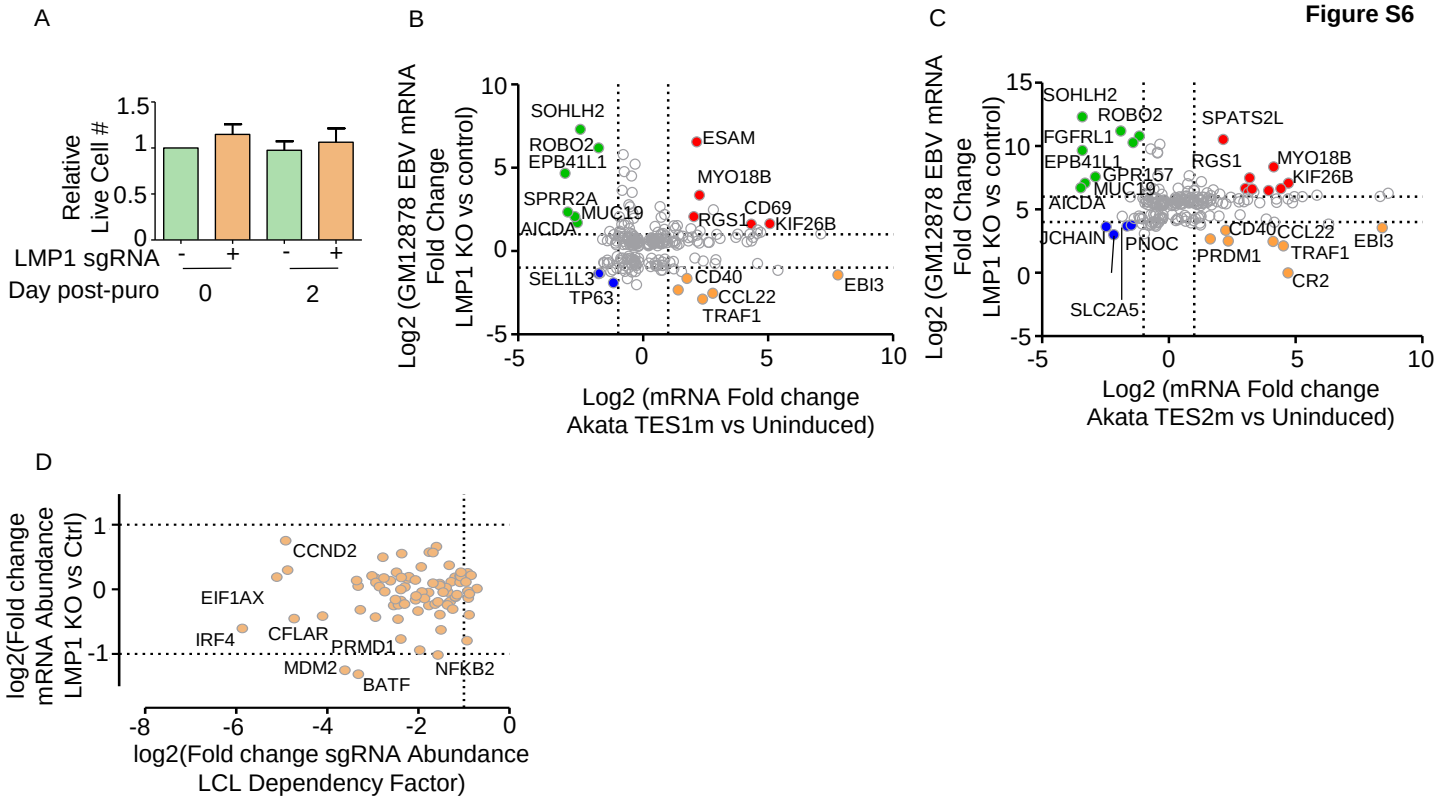
A
Relative Live Cell #
1.5
1
0.5
0
LMP1 sgRNA
-
+
-
+
Day post-puro
0
2
B
Log2 (GM12878 EBV mRNA Fold Change LMP1 KO vs control)
SOHLH2
ROBO2
EPB41L1
SPRR2A
MUC19
AICDA
SEL1L3
TP63
ESAM
MYO18B
CD69
RGS1
KIF26B
CD40
CCL22
TRAF1
EBI3
Log2 (mRNA Fold change Akata TES1m vs Uninduced)
C
Log2 (GM12878 EBV mRNA Fold Change LMP1 KO vs control)
SOHLH2
ROBO2
FGFRL1
EPB41L1
GPR157
MUC19
AICDA
JCHAIN
PNOC
SLC2A5
SPATS2L
RGS1
MYO18B
KIF26B
CD40
CCL22
PRDM1
TRAF1
EBI3
CR2
Log2 (mRNA Fold change Akata TES2m vs Uninduced)
D
log2(Fold change mRNA Abundance LMP1 KO vs Ctrl)
CCND2
EIF1AX
IRF4
CFLAR
PRMD1
MDM2
BATF
NFKB2
log2(Fold change sgRNA Abundance LCL Dependency Factor)

Fig. S6. CRISPR LMP1 KO effects on GM12878 LCL target gene regulation.

(A) Relative mean + SD live cell numbers from CellTitreGlo analysis of n=3 replicates of Cas9+ GM12878 LCL expressing control or LMP1 sgRNAs and puromycin selected for 0 vs 2 days.

(B) Scatter plot analysis cross comparing mRNA abundance fold changes in LMP1 sgRNA vs control (Y-axis) versus Akata expressing LMP1 TES1m for 24 hours vs uninduced (x-axis). Shown are genes differentially regulated by >1 fold.

(C) Scatter plot analysis cross comparing mRNA abundance fold changes in LMP1 sgRNA vs control (Y-axis) versus Akata expressing LMP1 TES2m for 24 hours vs uninduced (x-axis). Shown are genes differentially regulated by >1 fold.

(D) Scatter plot analysis cross comparing Log2 Fold change of GM12878 with LMP1 vs control sgRNA (Y-axis) versus CRISPR LCL vs Burkitt cell dependency factor analysis from (25) (X-axis). Shown are genes whose abundances changed by >1 fold in LMP1 KO vs control GM12878.

Figure 5

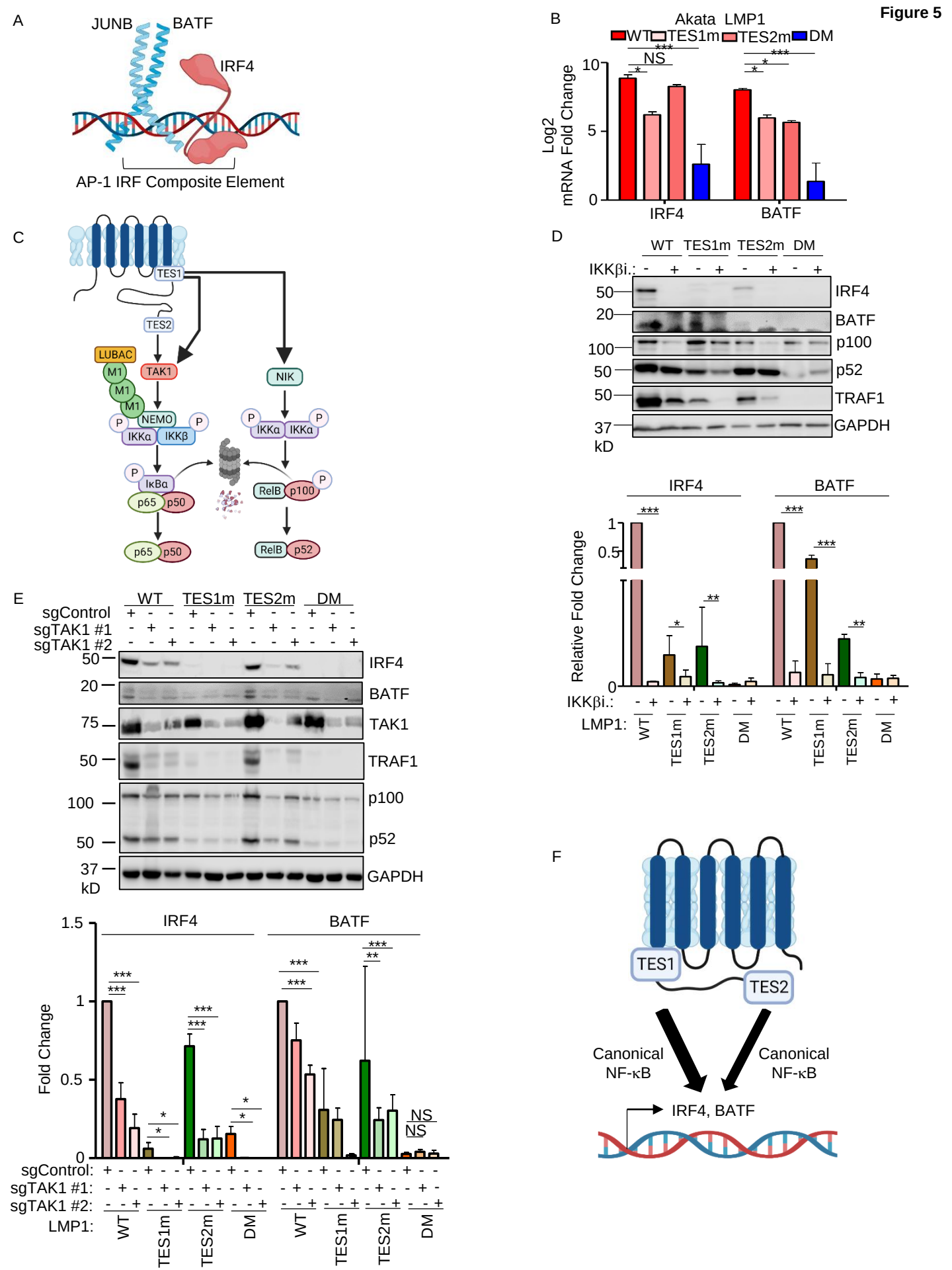
A
JUNB
BATF
IRF4
AP-1 IRF Composite Element
B
Akata LMP1
WT
TES1m
TES2m
DM
NS
Log2 mRNA Fold Change
IRF4
BATF
C
TES1
TES2
LUBAC
M1
TAK1
NEMO
IKKα
IKKβ
NIK
IKKα
IKKα
IκBα
p65
p50
RelB
p100
p52
D
WT
TES1m
TES2m
DM
IKKβi.:
IRF4
BATF
p100
p52
TRAF1
GAPDH
kD
Relative Fold Change
LMP1:
E
sgControl
sgTAK1 #1
sgTAK1 #2
TAK1
Fold Change
F
TES1
TES2
Canonical NF-κB
Canonical NF-κB
IRF4, BATF

Fig. 5 Roles of TES1 and TES2 canonical NF-κB pathways in LCL dependency factor BATF and IRF4 induction.

(A) Schematic diagram of JUNB, BATF and IRF4 at an AP-1/IRF composite DNA site.

(B) Log2 Fold changes + SD of IRF4, BATF and JUNB mRNA abundances from n=3 RNAseq replicates of Akata expressing the indicated LMP1 construct for 24 hours, as in Fig. 1. p-values were determined by one-sided Fisher's exact test. *$p<0.05$, ***$p<0.001$.

(C) Schematic diagram of LMP1 TES1 and TES2 NF-kB signaling. TES1 and TES2 can each activate canonical NF-κB pathways.

(D) Immunoblot analysis of WCL from Akata cells induced for LMP1 expression by 250 ng/ml doxycycline for 24 hours, either without or with 1 mM IKKβ inhibitor VIII for 24 hours. Shown below are relative foldchanges + SD of IRF4 or BATF vs GAPDH load control densitometry values from n=3 replicates, with values in vehicle control treated WT LMP1 expressing cells set to 1. P-values were determined by one-sided Fisher's exact test. **$p<0.001$, ***$p<0.0001$.

(E) Immunoblot analysis of WCL from Akata cells expressing control or either of two *TAK1* targeting sgRNAs, induced for LMP1 expression by 250 ng/ml doxycycline for 24 hours. Shown below are relative foldchanges + SD of IRF4 or BATF vs GAPDH load control densitometry values from n=3 replicates, with values in sgControl/WT LMP1 expressing cells set to 1. **$p<0.001$, ***$p<0.0001$.

(F) Model of additive TES1 and TES2 effects on BATF and IRF4 induction.

Figure S7

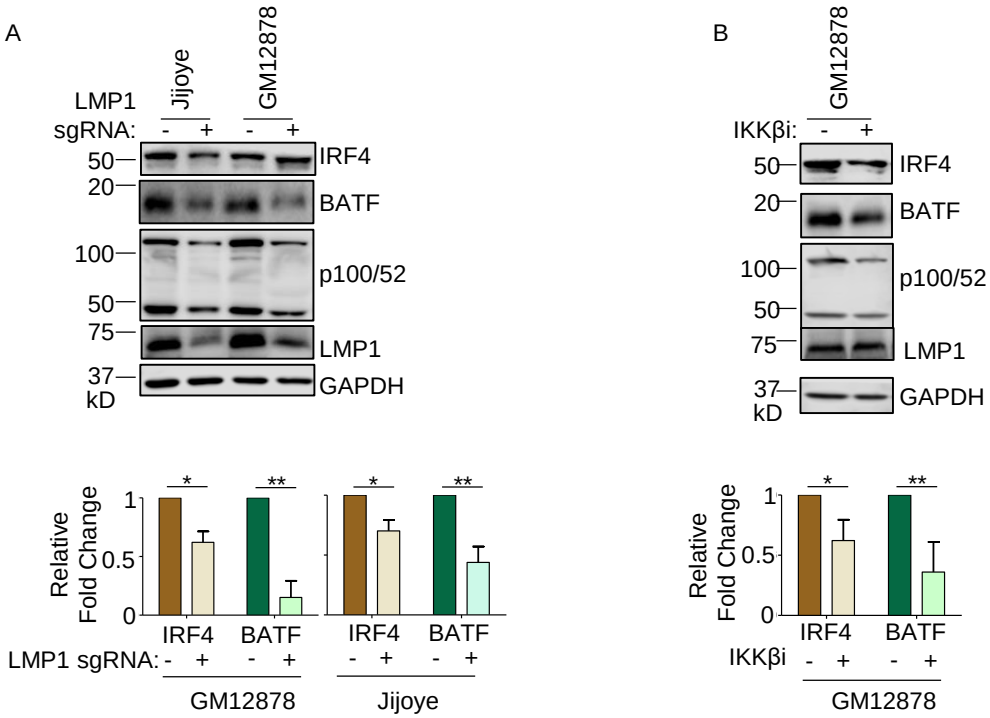
A
Jijoye
GM12878
LMP1
sgRNA: - + - +
50
20
IRF4
BATF
100
50
p100/52
75
LMP1
37
kD
GAPDH
Relative Fold Change
1
0.5
0
*
**
IRF4
BATF
LMP1 sgRNA: - + - +
GM12878
Jijoye
B
GM12878
IKKβi: - +
IRF4
BATF
p100/52
LMP1
GAPDH
IKKβi
GM12878

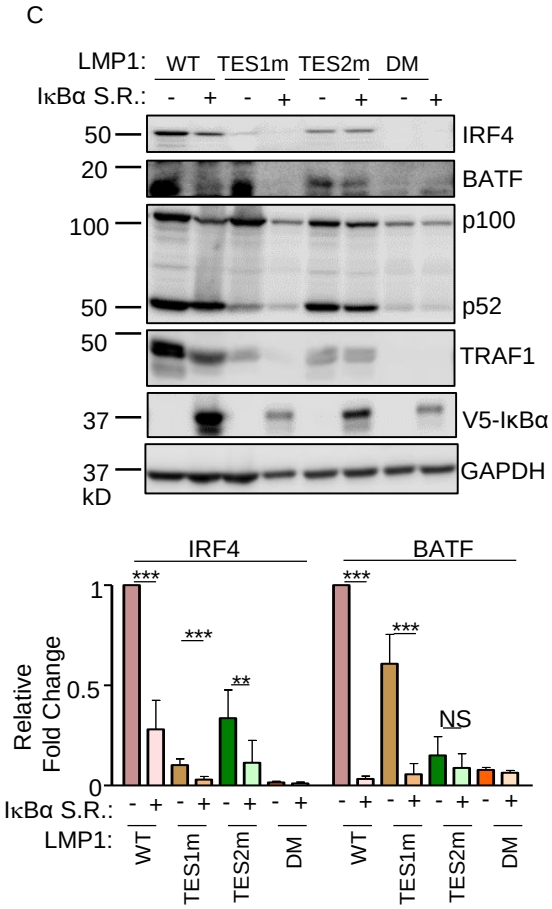
C
LMP1: WT TES1m TES2m DM
IκBα S.R.: - + - + - + - +
50
20
IRF4
BATF
100
p100
50
p52
50
TRAF1
37
V5-IκBα
37
kD
GAPDH
IRF4
BATF
Relative Fold Change
1
0.5
0
***
**
NS
IκBα S.R.: - + - + - + - + - + - + - + - +
LMP1: WT TES1m TES2m DM WT TES1m TES2m DM

Fig. S7 Roles of TES1 and TES2 canonical NF-κB pathways in BATF and IRF4 induction.

(A) Immunoblot analysis of WCL from latency III Jijoye Burkitt cells or GM12878 LCL expressing control or a *LMP1* targeting sgRNA. Shown below are relative foldchanges + SD of IRF4 or BATF vs GAPDH load control densitometry values from n=3 replicates, with values in sgControl expressing cells set to 1. P-values were determined by one-sided Fisher's exact test. **p<0.001, ***p<0.0001.

(B) Immunoblot analysis of WCL from GM12878 cells treated with vehicle control or 1 mM IKKβ inhibitor VIII for 24 hours. Shown below are relative foldchanges + SD of IRF4 or BATF vs GAPDH load control densitometry values from n=3 replicates, with values in vehicle control treated WT LMP1 expressing cells set to 1. P-values were determined by one-sided Fisher's exact test. **p<0.001, ***p<0.0001.

(C) Immunoblot analysis of WCL from Akata cells induced for the indicated LMP1 construct expression, either without or together with an IκBα super-repressor (IκBα-S.R.) that blocks canonical NF-kB signaling. Shown below are relative foldchanges + SD of IRF4 or BATF vs GAPDH load control densitometry values from n=3 replicates, with values in cells expressing WT LMP1 but not IκBα - set to 1. P-values were determined by one-sided Fisher's exact test. **p<0.001, ***p<0.0001.

Figure 6

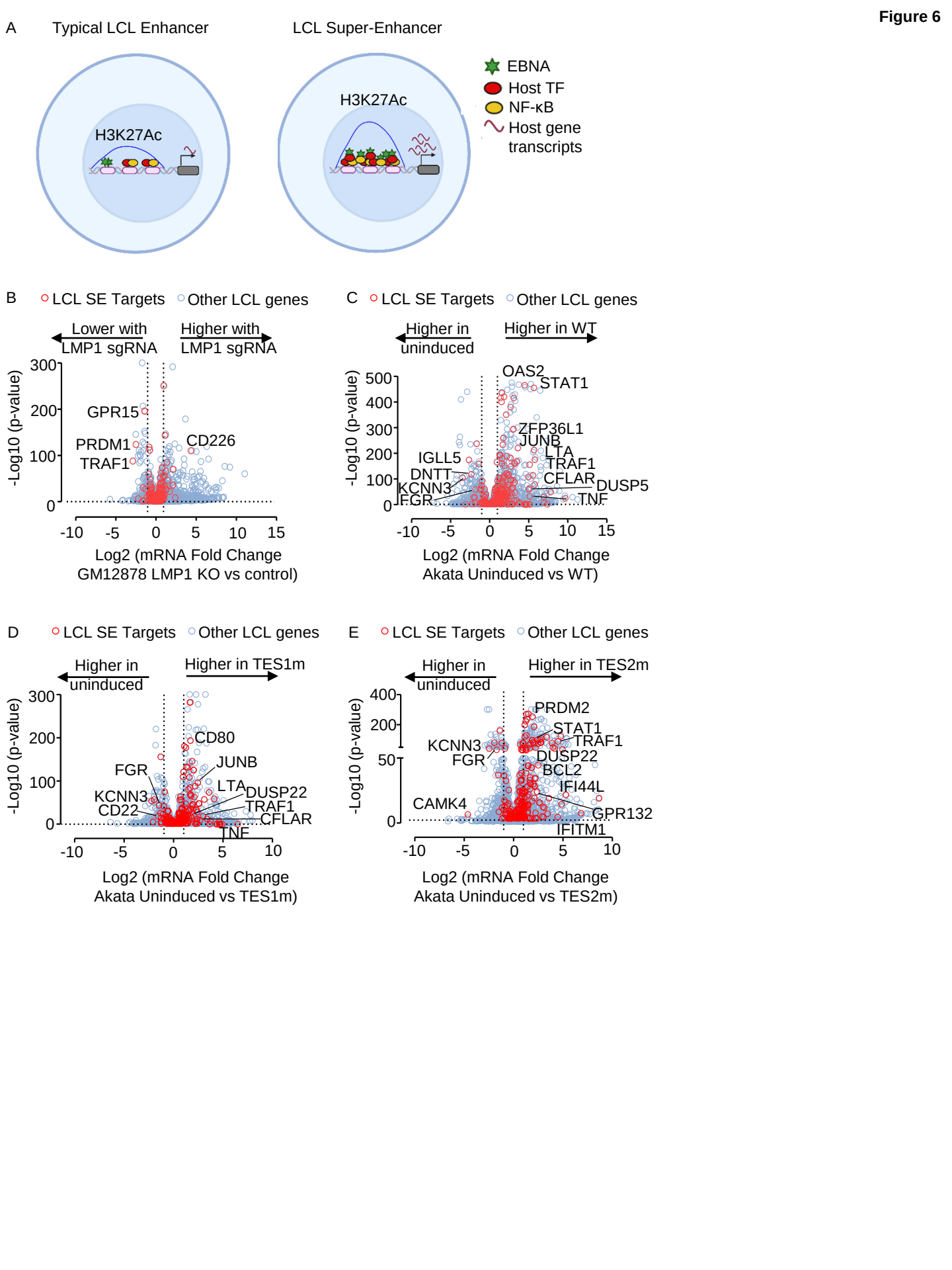
A
Typical LCL Enhancer
LCL Super-Enhancer
H3K27Ac
H3K27Ac
EBNA
Host TF
NF-κB
Host gene transcripts
B
LCL SE Targets
Other LCL genes
Lower with LMP1 sgRNA
Higher with LMP1 sgRNA
-Log10 (p-value)
GPR15
PRDM1
TRAF1
CD226
Log2 (mRNA Fold Change GM12878 LMP1 KO vs control)
C
LCL SE Targets
Other LCL genes
Higher in uninduced
Higher in WT
OAS2
STAT1
ZFP36L1
JUNB
LTA
TRAF1
CFLAR
DUSP5
TNF
IGLL5
DNTT
KCNN3
FGR
Log2 (mRNA Fold Change Akata Uninduced vs WT)
D
LCL SE Targets
Other LCL genes
Higher in uninduced
Higher in TES1m
CD80
JUNB
FGR
LTA
DUSP22
KCNN3
CD22
TRAF1
CFLAR
TNF
Log2 (mRNA Fold Change Akata Uninduced vs TES1m)
E
LCL SE Targets
Other LCL genes
Higher in uninduced
Higher in TES2m
PRDM2
STAT1
TRAF1
KCNN3
FGR
DUSP22
BCL2
IFI44L
CAMK4
GPR132
IFITM1
Log2 (mRNA Fold Change Akata Uninduced vs TES2m)

Fig. 6 LMP1 TES1 and TES2 roles in EBV super-enhancer target gene regulation in GM12878 LCL and Akata B-cell.

(A) Schematic diagram of typical LCL enhancers vs super-enhancers. Super-enhancers have significantly broader and taller histone 3 lysine 27 acetyl (H3K27Ac) peaks and are bound by all five LMP1-activated NF-κB transcription factor subunits, EBNA-2, LP, 3A, and 3C.

(B) Volcano plot of mRNA values in GM12878 expressing LMP1 vs control sgRNAs as in **Fig. 4F**. Genes targeted by EBV super-enhancers (SE) are highlighted by red circles, whereas other LCL genes are indicated by blue circles. P value cutoff of <0.05 and >1-fold gene expression were used.

(C) Volcano plot analysis of Akata RNA-seq, comparing mRNA values in cells induced for LMP1 WT vs. mock-induced for 24 hours, as in **Fig. 2A**. SE targeted genes highlighted by red circles and other B-cell genes indicated by blue circles. P value cutoff of <0.05 and >1-fold gene expression were used.

(D) Volcano plot analysis of Akata RNA-seq, comparing mRNA values in cells induced for LMP1 TES1m vs. mock-induced for 24 hours, as in **Fig. 2C**. SE targeted genes highlighted by red circles and other B-cell genes indicated by blue circles. P value cutoff of <0.05 and >1-fold gene expression were used.

(E) Volcano plot analysis of Akata RNA-seq, comparing mRNA values in cells induced for LMP1 TES2m for 24 hours vs. mock-induced, as in **Fig. 2E.** SE targeted genes highlighted by red circles and other B-cell genes indicated by blue circles. P value cutoff of <0.05 and >1-fold gene expression were used.

Figure S8

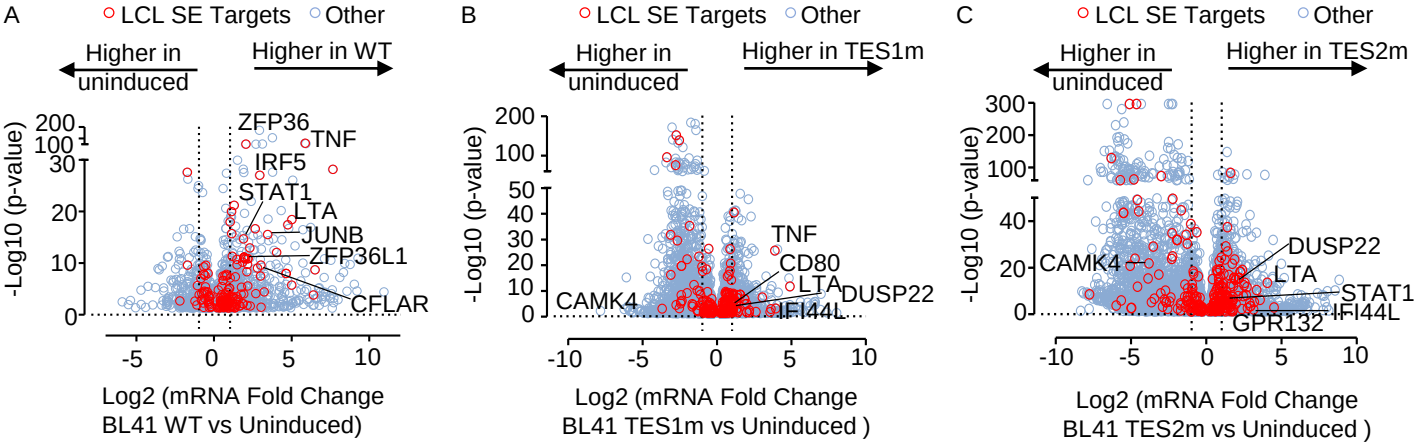
A
LCL SE Targets
Other
Higher in uninduced
Higher in WT
-Log10 (p-value)
ZFP36
TNF
IRF5
STAT1
LTA
JUNB
ZFP36L1
CFLAR
Log2 (mRNA Fold Change BL41 WT vs Uninduced)
B
LCL SE Targets
Other
Higher in uninduced
Higher in TES1m
-Log10 (p-value)
TNF
CD80
LTA
DUSP22
CAMK4
IFI44L
Log2 (mRNA Fold Change BL41 TES1m vs Uninduced)
C
LCL SE Targets
Other
Higher in uninduced
Higher in TES2m
-Log10 (p-value)
DUSP22
CAMK4
LTA
STAT1
IFI44L
GPR132
Log2 (mRNA Fold Change BL41 TES2m vs Uninduced)

Fig. S8 LMP1 TES1 and TES2 roles in EBV super-enhancer target gene regulation in BL-41 B-cell.

(A) Volcano plot analysis of BL-41 RNA-seq, comparing mRNA values in cells induced for LMP1 WT vs. mock-induced for 24 hours as in **Fig. S4A**. SE targeted genes highlighted by red circles and other B-cell genes indicated by blue circles. P value cutoff of <0.05 and >1-fold gene expression were used.

(B) Volcano plot analysis of BL-41 RNA-seq, comparing mRNA values in cells induced for LMP1 TES1m vs. mock-induced for 24 hours as in **Fig. S4C**. SE targeted genes highlighted by red circles and other B-cell genes indicated by blue circles. P value cutoff of <0.05 and >1-fold gene expression were used.

(C) Volcano plot analysis of BL-41 RNA-seq, comparing mRNA values in cells induced for LMP1 TES2m vs. mock-induced for 24 hours as in **Fig. S4E**. SE targeted genes highlighted by red circles and other B-cell genes indicated by blue circles. P value cutoff of <0.05 and >1-fold gene expression were used.

Figure 7

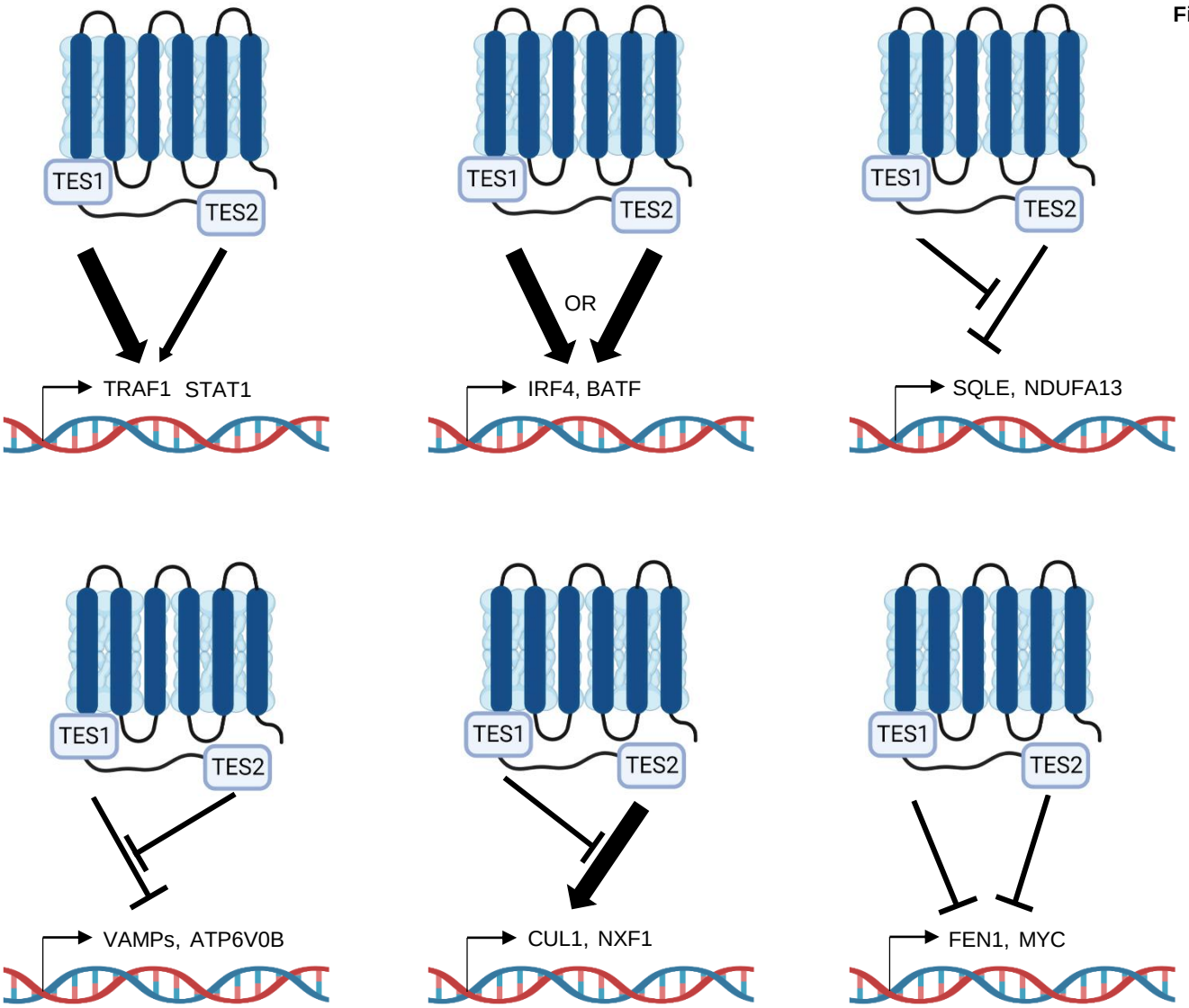
TES1
TES2
TRAF1 STAT1
TES1
TES2
OR
IRF4, BATF
TES1
TES2
SQLE, NDUFA13
TES1
TES2
VAMPs, ATP6V0B
TES1
TES2
CUL1, NXF1
TES1
TES2
FEN1, MYC

Fig. 7 Model highlighting different modes of LMP1 TES1 and TES2 cross-talk in B-cell target gene regulation.